Supplemental material to this article can be found at:
http://molpharm.aspetjournals.org/content/suppl/2021/08/01/molpharm.121.000280.DC1
1521-0111/100/3/295–307$35.00 https://doi.org/10.1124/molpharm.121.000280
MOLECULAR PHARMACOLOGY Mol Pharmacol 100:295–307, September 2021

Dynamic Expression of Transient Receptor Potential Vanilloid-3 and Integrated Signaling with Growth Factor Pathways during Lung Epithelial Wound Repair following Wood Smoke Particle and Other Forms of Lung Cell Injury[S]

Katherine L. Burrell, Nam D. Nguyen, Cassandra E. Deering-Rice, Tosifa A. Memon, Marysol Almestica-Roberts, Emmanuel Rapp, Samantha N. Serna, John G. Lamb, and Christopher A. Reilly

Department of Pharmacology and Toxicology, Center for Human Toxicology, University of Utah, Salt Lake City, Utah

Received March 19, 2021; accepted June 25, 2021

ABSTRACT

Prior studies revealed increased expression of the transient receptor potential vanilloid-3 (TRPV3) ion channel after wood smoke particulate matter (WSPM) treatment of human bronchial epithelial cells (HBECs). TRPV3 attenuated pathologic endoplasmic reticulum stress and cytotoxicity mediated by transient receptor potential ankyrin-1. Here, the basis for how TRPV3 expression is regulated by cell injury and the effects this has on HBEC physiology and WSPM-induced airway remodeling in mice was investigated. TRPV3 mRNA was rapidly increased in HBECs treated with WSPM and after monolayer damage caused by tryptic disruption, scratch wounding, and cell passaging. TRPV3 mRNA abundance varied with time, and stimulated expression occurred independent of new protein synthesis. Overexpression of TRPV3 in HBECs reduced cell migration and wound repair while enhancing cell adhesion. This phenotype correlated with disrupted mRNA expression of ligands of the epidermal growth factor, tumor growth factor-β, and frizzled receptors. Accordingly, delayed wound repair by TRPV3 overexpressing cells was reversed by growth factor supplementation. In normal HBECs, TRPV3 upregulation was triggered by exogenous growth factor supplementation and was attenuated by inhibitors of growth factor receptor signaling. In mice, subacute oropharyngeal instillation with WSPM also promoted TRPV3 mRNA expression and epithelial remodeling, which was attenuated by TRPV3 antagonist pre- and cotreatment. This latter effect may be the consequence of antagonist-induced TRPV3 expression. These findings provide insights into the roles of TRPV3 in lung epithelial cells under basal and dynamic states, as well as highlight potential roles for TRPV3 ligands in modulating epithelial damage/repair.

SIGNIFICANCE STATEMENT

Coordinated epithelial repair is essential for the maintenance of the airways, with deficiencies and exaggerated repair associated with adverse consequences to respiratory health. This study shows that TRPV3, an ion channel, is involved in coordinating repair through integrated repair signaling pathways, wherein TRPV3 expression is upregulated immediately after injury and returns to basal levels as cells complete the repair process. TRPV3 may be a novel target for understanding and/or treating conditions in which airway/lung epithelial repair is not properly orchestrated.

This work was supported by National Institutes of Health National Institute of Environmental Health Sciences (NIEHS) [R01 ES017431 and R01 ES027015]. K.L.B. received partial support from a University of Utah Associated Regional and University Pathologists (ARUP) fellowship and the Skaggs Graduate Research Fellowship. N.D.N. was supported in part by a University of Utah Undergraduate Opportunities award, and M.A.R. by a National Institutes of Health National Institute of General Medical Sciences (NIGMS) Diversity Supplement award [R01 GM121648].

The authors declare no conflicts of interest.

https://doi.org/10.1124/molpharm.121.000280.

[S] This article has supplemental material available at molpharm.aspetjournals.org.

Introduction

Particulate matter (PM) derived from burning wood and biomass (WSPM) is a specific and pervasive type of air pollutant. WSPM exposure is associated with increased rates of hospital admissions for respiratory complications (Swiston et al., 2008; Ghio et al., 2012; Reid et al., 2016; Liu et al., 2017), whereas long-term exposure causes and exacerbates chronic diseases

ABBREVIATIONS: 007, 2-(5-trifluoromethyl-pyridine-2ylsulfanyl)-1-(8-methyl-3,4-dihydro-2H-quinolin-1-yl)-ethanone; 008, (*S*)-(1-(3,4-dichlorophenyl)cyclobutyl)(pyridin-2-yl)methanol; ActD, actinomycin D; AREG, amphiregulin; ATCC, American Type Culture Collection; B2BV3OE, BEAS-2B cells stably overexpressing TRPV3; BEAS-2B, human bronchial epithelial cells; CHX, cycloheximide; DPTHF, diphenyltetrahydrofuran; EGFR/ErbB1, epidermal growth factor receptor; EMT, epithelial-to-mesenchymal; EPGN, epithelial mitogen; ErbB2, HER2/receptor tyrosine kinase 2; ErbB3, HER3/receptor tyrosine kinase 3; Fz, Frizzled; FZD5, frizzled class receptor 5; GSK3β, glycogen synthase kinase 3β; HBEC, human bronchial epithelial cell; HB-EGF, heparin-binding EGF-like growth factor; JNK, mitogen-activated protein kinase 8; LHC-9, Lechner and LaVeck media; NF-κB, nuclear factor κB; NRG1, neuregulin 1; OPA, oropharyngeal aspiration; p38 MAPK, mitogen-activated protein kinase 14; PM, particulate matter; qPCR, quantitative real-time polymerase chain reaction; TGFα, transforming growth factor α; TGFβ1, transforming growth factor β1; TGFβ2, transforming growth factor β2; TGFβR, transforming growth factor receptor β; TRPA1, transient receptor potential ankyrin-1; TRPV3, transient receptor potential vanilloid-3; TRPV3KO, HBEC3-KT where TRPV3 has been knocked out; Wnt, wingless-type MMTV integration site family; WSPM, wood smoke particulate matter.

including asthma and chronic obstructive pulmonary disorder (Laumbach and Kipen, 2012; Olloquequi and Silva O, 2016).

How WSPM affects the respiratory tract is not fully understood. Our laboratory demonstrated that pine, mesquite, and other biomass smoke PM activate the transient receptor potential ankyrin-1 (TRPA1) and vanilloid-3 (TRPV3) ion channels (Shapiro et al., 2013; Deering-Rice et al., 2018). Activation of TRPA1 by WSPM in human bronchial epithelial cells (HBECs) causes endoplasmic reticulum Ca^{2+} depletion and activation of the eukaryotic translation initiation factor 2-α kinase-3–dependent branch of the endoplasmic reticulum stress response. This pathway promotes proapoptotic DNA damage-inducible transcript-3 expression and cell death. Additionally, pine and other forms of WSPM, pure TRPA1 agonists, and diesel exhaust particles stimulate the expression and secretion of gel-forming mucins 5AC and 5B and the EGFR ligand cell surface–associated mucin 4 in HBECs (Deering-Rice et al., 2019; Memon et al., 2020).

The consequences of TRPV3 activation in HBECs by WSPM and other substances are not fully understood. The discovery that TRPV3 expression increases in HBECs after treatment with cytotoxic concentrations of WSPM and TRPA1 agonists, and that TRPV3 counteracts TRPA1 activity, endoplasmic reticulum stress, and cytotoxicity, provides clues that TRPV3 may be critical for adaptation of lung epithelial cells to cytotoxic insults (Nguyen et al., 2020). This idea is further supported by the finding that TRPV3 inhibition prevented increases in airway resistance in WSPM-treated mice, via an unknown mechanism (Deering-Rice et al., 2018).

TRPV3 is important in cutaneous physiology and plays roles in pain, itch, hair growth, and skin homeostasis (Cheng et al., 2010; Yang et al., 2017). TRPV3 is necessary for regulated keratinocyte proliferation and the formation and maintenance of the skin barrier, including terminal differentiation of the epidermis (Borbíró et al., 2011). Knockout of *Trpv3* in mice reduces terminal differentiation and barrier integrity and promotes a curly hair morphology, in part, by interactions with the TGFα/EGFR signaling nexus (Cheng et al., 2010). There have been no pulmonary phenotypes associated with *Trpv3* knockout. Alternatively, low-level TRPV3 activation may stimulate cell growth, whereas overstimulation of TRPV3 inhibits proliferation and induces apoptosis. Of note, the congenital disorder Olmsted syndrome is caused by rare mutations rendering TRPV3 constitutively active, leading to palmoplantar keratoderma, perioral keratotic plaques, and severe itching at lesions (Lin et al., 2012). These morbidities can be attributed to the fragility of the epithelium, in which overgrowth of keratinocytes serves as protection, manifesting as hyperkeratosis (McLean and Irvine, 2007). Also, no pulmonary phenotypes have been associated with Olmsted syndrome.

TRPV3 may have similar roles in the lung epithelium. The airway epithelium is the first line of defense against environmental insults such as inhaled particles, pathogens, and toxic chemicals, and it is a common site of damage by inhaled pneumotoxicants. Improper control of inflammation and resolution of repair can promote airway remodeling and adverse health outcomes (Zemans et al., 2013). The initial stages of epithelial repair are crucial, and include dedifferentiation, spreading, and proliferation of epithelial cells adjacent to the wound. Immediate changes in ATP, H_2O_2, and Ca^{2+} stimulates, in a spatially and temporally limited manner, the expression of genes needed for repair. Receptor tyrosine kinases are also activated by pre-existing and transcriptionally induced growth factors, and chemokines that signal surrounding cells to engage in the repair process (Cordeiro and Jacinto, 2013). Studies using different tissues have found that voltage-gated Ca^{2+} channels, including transient receptor potential channels, become induced and are critical in maintaining Ca^{2+} homeostasis (Cordeiro and Jacinto, 2013). For example, transient receptor potential canonical-1 (Fabian et al., 2008), transient receptor potential vanilloid-2 (Monet et al., 2009), transient receptor potential vanilloid-4 (Fiorio Pla et al., 2012; Martin et al., 2012), transient receptor potential melastatin-7 (Middelbeek et al., 2015), and transient receptor potential melastatin-8 (Wondergem and Bartley, 2009) regulate cell migration in various cell types. How TRPV3 responds to cell injury and influences epithelial repair in the lungs is not known.

Here, it was postulated that TRPV3 helps coordinate repair in HBECs. It is shown that synchronized expression of TRPV3 is essential for epithelial repair after WSPM-induced and other forms of injury in vitro and in mouse airways. The results provide new insights into mechanisms by which TRPV3 may regulate WSPM injury and highlight possibilities for using TRPV3 ligands to modulate lung injury and repair.

Materials and Methods

Chemicals. Unless specified, chemicals were purchased from Sigma-Aldrich (St. Louis, MO). The inhibitors CP-724714 (ErbB2) and PD169316 (p38 MAPK) were purchased from Cayman Chemical (Ann Arbor, MI). AG-1478 (ErbB1/EGFR) was purchased from Selleckchem.com (Houston, TX). AZD 8931 (EGFR, ErbB2, ErbB3) was purchased from APExBIO (Houston, TX), and TWS119 (GSK3β) and SP600125 (JNK) from ChemCruz (Dallas, TX). Afatinib dimaleate (EGFR, ErbB2, HER4/receptor tyrosine kinase 4), IWP 2 (inhibitor of Wnt production 2, targeting porcupine), SB 431542 (TGFβRI), and ITD 1 (1,4-dihydropyridine inducer of TGFβRII degradation-1) were purchased from Tocris (Minneapolis, MN). Recombinant human heparin-binding EGF-like growth factor (HB-EGF), epigen (EPGN), neuregulin 1 (NRG1), amphiregulin (AREG), recombinant human transforming growth factor β2 (TGFβ2), and recombinant human secreted frizzled related protein-1 were purchased from R&D Systems (Minneapolis, MN). Recombinant human transforming growth factor β1 (TGFβ1) was purchased from Abcam (Cambridge, United Kingdom) and Wnt7a from PeproTech (Rocky Hill, NJ). All recombinant human proteins were reconstituted and stored according to supplier recommendations. The TRPV3 antagonists 2-(5-trifluoromethyl-pyridine-2ylsulfanyl)-1-(8-methyl-3,4-dihydro-2H-quinolin-1-yl)-ethanone (referred to hereafter as 007) and (*S*)-(1-(3,4-dichlorophenyl)cyclobutyl)(pyridin-2-yl)methanol [referred to hereafter as 008; also known as 5a (Gomtsyan et al., 2016)] were synthesized as previously described (Deering-Rice et al., 2014) by the University of Utah Synthetic and Medicinal Chemistry Core. The purified products were verified by mass spectrometry, ^{1}H NMR, and ^{13}C NMR.

Cells. HBEC3-KT cells (ATCC, Rockville, MD) (Delgado et al., 2011) were grown in Airway Epithelial Basal Medium supplemented with Bronchial Epithelial Cell Growth Kit (ATCC, Rockville, MD). BEAS-2B cells (ATCC, Rockville, MD) were grown in LHC-9. Human TRPV3 overexpressing BEAS-2B cells (B2BV3OE) were generated as previously described (Deering-Rice et al., 2018). All cells were cultured in a humidified incubator at 37°C with a 95% air:5% CO_2 atmosphere and regularly passaged using trypsin before becoming 100% confluent.

In Vitro Injury Models. Cells were injured using four different processes: 1) cell passaging injury was performed by washing confluent cells with PBS, adding trypsin [TrypLE Express Enzyme (1X), ThermoFisher], and incubating at 37°C for 5 minutes, dislodging cells, and replating cells; 2) trypsin injury was performed by incubating cells with trypsin (TrypLE Express, Invitrogen; Carlsbad, CA) for 1 minute, removal of the trypsin, and monitoring under a light microscope until the monolayer was disrupted (i.e., cells were slightly rounded, and cell-cell contacts were lost; ~3–5 minutes depending upon cell type). Fresh media was then added; 3) mechanical injury in the form of a scratch wound created using a grid pattern was made using a pipette tip, washed twice with PBS to remove the nonadherent cells, and adding fresh media; and 4) cytotoxic injury, which involved treatment of monolayers with a cytotoxic (~50% cell death with 24-hour treatment) concentration of pine WSPM (0.076 mg/ml equivalent to 20 $\mu g/cm^2$), which also disrupts the monolayer. These methods were chosen for purposes of studying mechanisms of WSPM injury, as well as to ascertain the relevance of findings in the context of a proteolytic mechanism of injury, as well as to simply understand how cells respond when attempting to reform a damaged epithelial layer.

Pine WSPM. Pine WSPM was generated as previously described (Deering-Rice et al., 2018). Approximately 10 g of dry Austrian pine, collected from a tree growing in the Salt Lake Valley, was burned in a laboratory furnace. PM was collected using an Anderson cascade impactor, and fraction 7 (F7; PM size: 0.43–0.65 μm) was resuspended in DMSO to an initial concentration of 115 mg/ml, or 500 mg/ml for in vitro and in vivo experiments, respectively. Pine WSPM was diluted further to the final working concentration of 0.076 mg/ml (20 $\mu g/cm^2$ in the 6-well treatment plates) in cell culture media, and 0.5 mg/ml, diluted in saline, for treatment of animals at a final dose of 0.5 mg/kg, as described below.

Quantitative Real-Time Polymerase Chain Reaction. Total RNA was isolated from cells using the PureLink RNA Mini Kit (Invitrogen; Carlsbad, CA). For time course experiments, cells were subjected to cell passaging injury. Cells were typsinized, and 1/2 of the cells were immediately collected for the t = 0 baseline time point. The remaining cells were plated in 6-well plates for temporal gene expression studies. cDNA was synthesized from 2 μg of total RNA using the ABI High-Capacity cDNA Synthesis Kit with RNase inhibitor (Applied Biosystems, Foster City, CA). The samples were probed for human TRPV3 mRNA (Hs00376854_m1) using TaqMan probes (Applied Biosystems). TaqMan probes for HB-EGF (Hs00181813_m1), EPGN (Hs02385424), AREG (Hs00950669), NRG1 (Hs01101538_m1), TGFβ1 (Hs00998133_m1), TGFβ2 (Hs00234244_m1), Wnt7a (Hs011149990_m1), ErbB1 (Hs01076090_m1), ErbB2 (Hs01001580_m1), ErbB3 (Hs00176538_m1), TGFβRI (Hs00610320_m1), TGFβRII (Hs00234253_m1), and FZD5 (Hs00258278_s1) were also used. Analysis by qPCR was performed using a Life Technologies QuantStudio 6 Flex instrument. Values for relative gene expression were normalized to the housekeeping gene β2-microglobulin (Hs00984230_m1), which exhibited stability across treatments, utilizing the comparative cycle threshold (ΔΔCT) method.

Ca^{2+} Flux Assay. Cells were plated in a 96-well plate (10,000 cells/well) and grown for either 24 or 84 hours. TRPV3-dependent Ca^{2+} flux was measured using the Fluo-4 Direct assay kit (Invitrogen; Carlsbad, CA). Fluo-4 AM was diluted in LHC-9, and the cells were loaded at room temperature (22 to 23°C) as previously described (Deering-Rice et al., 2011). Fluorescence micrographs were captured using the EVOS FL Auto microscope at 10X magnification with a GFP filter. After baseline fluorescence was captured, cells were treated with the TRPV3-selective agonist drofenine, prepared in LHC-9 medium (which contains 111.1 μM Ca^{2+}), at 3X concentration at room temperature. Images were captured immediately prior to treatment application and every 40 seconds thereafter, for 160 seconds. After agonist treatment, cells were treated with the Ca^{2+} ionophore, ionomycin (10 μM final concentration) in LHC-9 to determine the maximum attainable response and for normalization of the agonist-induced response. The change in fluorescence (i.e., Ca^{2+} content) was further normalized to blank LHC-9 media and quantified using an Image-J–based software.

Kinetic Scratch Wound Assays. Cells were plated at 25,000 cells/cm^2 and grown for 48 hours to 100% confluence on an Image-Lock 96-well culture plate (Essen BioSciences, Ann Arbor, MI). Precision mechanical scratch wounds were made using the Incucyte WoundMaker 96-pin wound-making tool (Essen BioSciences). The cells were then washed 2x with PBS to remove the detached cells, and then the desired treatments were added. Scratch wound closure images were captured at 1 hour intervals using an IncuCyte ZOOM real-time live-cell imaging system, which was housed in a climate-controlled cell culture incubator. Wound confluence was measured as the percent of the initial gap that was covered by migrating cells, and parameters were set and the image series analyzed using IncuCyte ZOOM software.

RNA Sequencing. Transcript profiling of BEAS-2B and B2BV3OE cells was performed by the High Throughput Genomics Core Facility at the Huntsman Cancer Institute, University of Utah, as described previously (Deering-Rice et al., 2018). Briefly, BEAS-2B and B2BV3OE cells were plated in T-25 flasks and grown to 100% confluence before RNA isolation. RNA was isolated using RNeasy kit with on-column DNase1 digestion (Qiagen). The Illumina TruSeq Stranded mRNA Sample Preparation Kit was used to generate the library, and the samples were analyzed using an Illumina HiSeq instrument (HCS v2.0.12 and RTA v1.17.21.3), with a 50-cycle single read sequence. Data were processed by the University of Utah Bioinformatics Core. The data presented in this publication have been deposited in the National Center for Biotechnology Information (NCBI) Gene Expression Omnibus (GEO) (Edgar et al., 2002) and are accessible through GEO Series accession number GSE109598.

Cell Adhesion Assay. BEAS-2B and B2BV3OE cells were passaged and plated at a density of 30,000 cells/cm^2 in a 96-well plate with fresh LHC-9 media and incubated for 2 hours. Nonadherent cells were removed with two PBS washes. Cell counting kit-8 (CCK-8) viability reagent (Dojindo, Rockville, MD) was diluted to 8% in LHC-9 media and then added to the culture wells to quantify adherent cells. After 2 hours incubation time at 37°C, the absorbance at 450 nm was determined using a plate reader. The number of adherent cells was calculated by comparing absorbance values to a standard curve of known cell seeding density/cell number plated and measured after the 2-hour incubation (without washing).

Mice. Experimental procedures were approved by the University of Utah Institutional Animal Care and Use Committee. Mice were housed in a vivarium with 12-hour light/dark cycles and provided standard chow and water ad libitum. Male and female 6–8 weeks old C57BL/6 mice weighing 20–25 g were used for subacute saline, pine WSPM, and TRPV3 antagonist (007) exposures. Both male and female mice were used to address sex as a variable, and no overt differences have been observed. Saline vehicle control or fresh pine WSPM (0.5 mg/kg in saline) was dosed via oropharyngeal aspiration (OPA) for a total of 3 times, every other day. After (24 hours) the third dose (day 6), mice were sacrificed, and the respiratory tissues collected. Rationale for this dosing paradigm has been previously described in detail (Deering-Rice et al., 2018). Mice were also injected intraperitoneally with the TRPV3 antagonist 007 at 1 mg/kg diluted in saline from a stock in DMSO (final DMSO = 1%) 1 hour prior to pine WSPM instillation. These mice were also cotreated with 007 (1 μM) diluted in the pine WSPM suspension or saline, via OPA, to ensure local inhibition of TRPV3 during the WSPM exposure. At 24 hours after the 3rd dose, mice were euthanized, and the lungs were inflated and fixed with 10% neutral-buffered formalin at a constant hydrostatic pressure of 25 cm H_2O. The left lobe of the lungs was dissected, mounted, sliced into serial 5-μm sections, and stained with trichrome for histologic analysis by the University of Utah Research Histology Core. Lungs from additional mice within the same treatment groups were also inflated with RNA later and stored at 4°C. The lungs were then microdissected, separating the upper airways

(trachea and bronchi) from the smaller, lower airways and parenchymal tissue, and placed in TRIzol. The tissue was immediately homogenized and extracted with chloroform before further processing of the aqueous phase using the PureLink RNA Mini Kit (Invitrogen; Carlsbad, CA) to isolate total RNA. cDNA was synthesized from 2 μg of total RNA using the ABI High-Capacity cDNA Synthesis Kit with RNase inhibitor (Applied Biosystems, Foster City, CA). The samples were probed for mouse *Trpv3* mRNA (Mm00455003_m1) using TaqMan probes (Applied Biosystems). Analysis by qPCR was performed using a Life Technologies QuantStudio 6 Flex instrument. Values for relative gene expression were normalized to the housekeeping gene mouse glyceraldehyde-3-phosphate dehydrogenase mRNA (*Gapdh*, Mm99999915_g1), which exhibited stability across treatments, using the comparative cycle threshold (ΔΔCT) method. Some studies also used *Trpv3*$^{-/-}$ C57BL/6J mice. These mice were purchased from Jackson laboratories and were maintained on site, as described above.

TRPV3-Knockout HBEC3-KT Cells. The target sequence 5′-GCCGGATGTTGGAATCCAT-3′ was cloned into pX459-pSpCas9-2A-mCherry V2.0 [modified from Addgene, pSpCas9(BB)-2A-Puro V2.0] to coexpress Cas9-2A-mCherry protein and a guide RNA targeting TRPV3 at exon 2. This sequence introduced a premature stop codon in the TRPV3 gene. Normal human bronchial epithelial cells immortalized with cyclin dependent kinase 4 (CDK4) and human telomerase reverse transcriptase (hTERT) were transfected with this construct using FuGENE 6 transfection reagent (Promega) at a 2:1 ratio of reagent to DNA in 250 μl OptiMEM media. To isolate stably modified cells, the cells were cultured, trypsinized, and sorted by flow cytometry using a BD FACSAria, collecting the top 1% of mCherry-expressing cells. Cells were then cultured and subjected to Fluorescence activated cell (FAC) sorting for 5 subsequent passages, isolating the top 1% of mCherry-positive cells in each sort as single cells to be expanded. On-target editing in the final cell line was verified by the University of Utah Mutation Generation and Detection Core Facility using tracking of indels by decomposition (TIDE) sequencing.

Statistical Analysis. Values are represented as the mean ± S.D. unless stated otherwise. For comparisons between two groups, the unpaired *t* test was used. One-way ANOVA with Dunnett's post-test was used for multiple comparisons, unless indicated otherwise. A P value < 0.05 was considered significant.

Results

TRPV3 mRNA and Protein/Function Increased in HBEC3-KT Cells after Multiple Types of Monolayer Injury. TRPV3 mRNA was quantified after different types of monolayer injury (Fig. 1A). Compared with the vehicle control, pine WSPM treatment increased TRPV3 expression ~20-fold ($P < 0.0001$), similar to that previously reported for primary lobar HBECs treated with pine WSPM (Nguyen et al., 2020). Likewise, cell passaging and trypsin digestion alone increased TRPV3 mRNA ~25- and 10-fold ($P < 0.0001$), respectively, whereas scratch wounded cells exhibited a ~4-fold increase in TRPV3 mRNA ($P = 0.0755$). The relatively limited change in TRPV3 mRNA in the mechanical/scratch wound model was attributed to less uniform/widespread monolayer damage. Supplemental Table 1 shows additional results for upregulation of TRPV3 mRNA using these injury models on other immortalized and primary HBEC cell lines.

After passaging injury, TRPV3 mRNA levels spiked at 2 hours and again at 18 hours, but as the cells re-established monolayer integrity and became confluent at ~72 hours postplating, the levels of TRPV3 mRNA returned to baseline (Fig. 1B). Differences in TRPV3 expression in relation to confluence was confirmed as changes in TRPV3-dependent Ca^{2+} flux, as a function of time after plating (Fig. 1C), as well as western blotting (Supplemental Fig. 1). Specifically, cells that were less confluent and actively proliferating (i.e., high TRPV3 mRNA expression; 24 hours postplating at ~20% confluence) exhibited greater responses to drofenine, a selective TRPV3 agonist (Deering-Rice et al., 2014), compared with 100% confluent cells (i.e., low TRPV3 mRNA expression; 84 hours postplating, $P < 0.0001$). This same time-dependent change in mRNA expression was observed in BEAS-2B cells and, to a much lesser extent, in B2BV3OE cells (Supplemental Fig. 2).

Rapid Increases in TRPV3 Transcription Did Not Require New Protein Synthesis. HBEC3-KT cells were subjected to passaging injury and treated for 2 hours with either 100 nM cycloheximide (CHX; a protein synthesis inhibitor), or 50 μM actinomycin D (ActD), a potent transcription inhibitor (Fig. 2). CHX treatment enhanced TRPV3 mRNA expression ~1.5-fold ($P = 0.001$). As expected, ActD treatment prevented an increase in TRPV3 expression ($P < 0.0001$).

Overexpression of TRPV3 Slows Migration and Wound Repair while Promoting Cell Adhesion. Figure 3A summarizes wound repair results after a mechanical/scratch. Representative live-cell microscopy images comparing the extent of wound repair at 45 hours are shown in Fig. 3B. These results show that stable overexpression of TRPV3 (B2BV3OE cells) interfered with the ability of cells (red line) to repair a scratch injury, with full repair occurring well after 48 hours. Conversely, BEAS-2B cells (black line) repaired scratch wounds within ~6 hours. A scratch mask (red) and confluent cell mask (teal) is overlaid on the images in Fig. 3B, to highlight the marked differences in wound closure. Time-lapse videos are also included as Supplemental Movie 1. In the movie, it was also noted that B2BV3OE cells were less mobile than BEAS-2B cells, moving more as a cohesive unit rather than individual cells migrating throughout the wound site.

Regulated cell adhesion is necessary for wound repair; too little or too much alters migration and repair potential (Crosby and Waters, 2010). As shown in Fig. 3, A and B, and Supplemental Movie 1, B2BV3OE cells remained mostly stationary after scratch wounding, and B2BV3OE cells were found to be more adherent within 2 hours of plating (Fig. 3C). To this end, it was also found that TRPV3OE cells expressed comparatively lower levels of the mesenchymal marker Vimentin, while having higher levels of expression of E-cadherin and F-actin (Supplemental Fig. 3). Additionally, TRPV3KO cells were ~20% less adherent than normal HBEC3-KT cells in an adhesion assay (data not shown).

Transcriptomic Comparisons of Normal and TRPV3 Overexpressing Cells Suggested Integration of TRPV3 with Canonical Growth Factor Signaling Pathways. Transcriptomic analysis (Fig. 4A) revealed lower levels of transcripts for multiple growth factors related to EGFR/ErbB1–3 signaling, as well as Wnt7a and TGFβ1 in B2BV3OE cells, but negligible differences in ErbB1–3, TGFβRI, and Frizzled-5 (FZD5, activated by Wnt7a) receptors. qPCR analysis was also performed to confirm the transcriptomic results (Fig. 4, B and C). As expected, EPGN, AREG, NRG1, HB-EGF, and Wnt7a were all downregulated in B2BV3OE cells. However, TGFβ2 was upregulated. TGFβ1 appeared to be slightly lower in

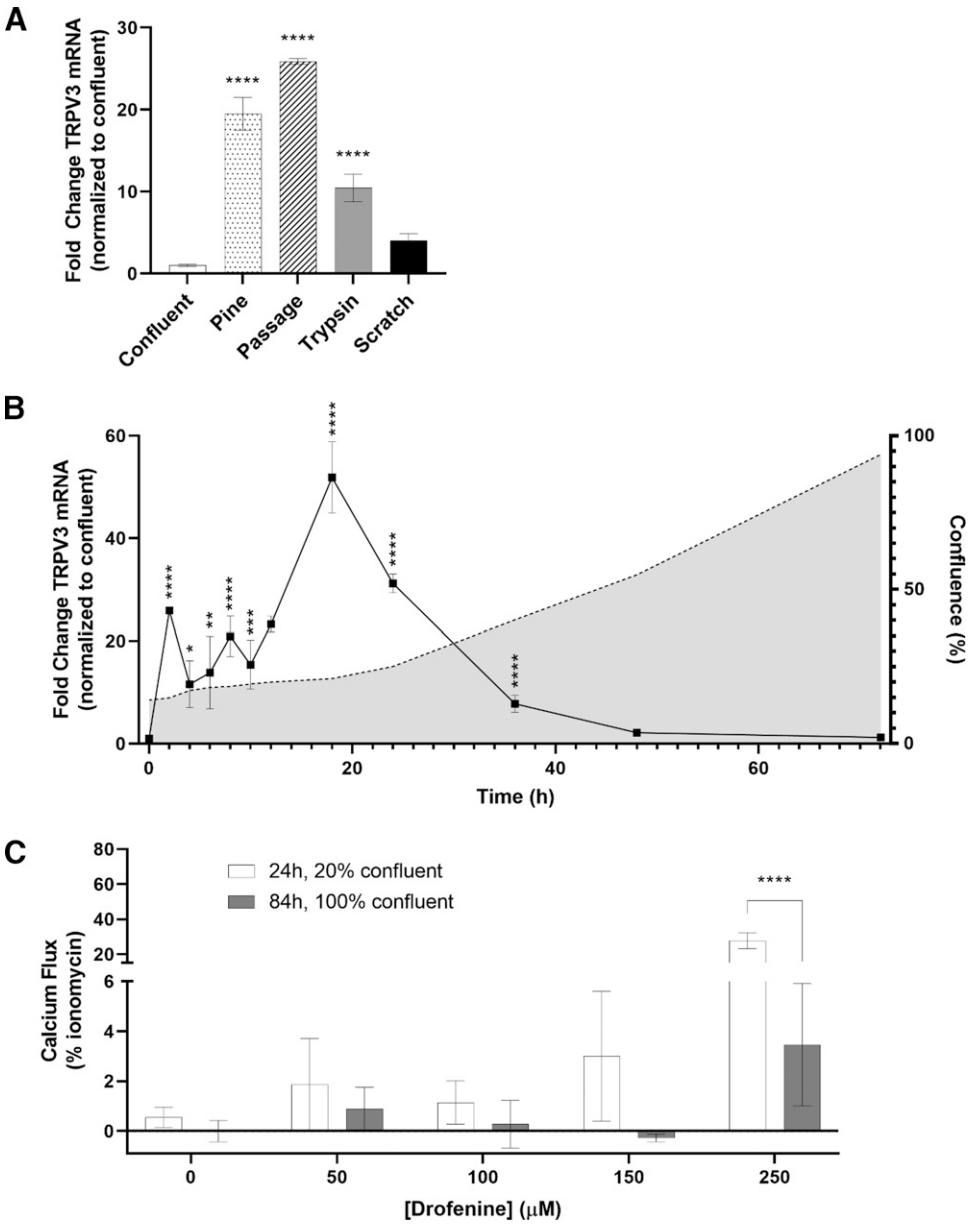

Fig. 1. TRPV3 expression increased following epithelial injury in vitro. (A) TRPV3 expression in HBEC3-KT cells after four different in vitro models of barrier disruption: 0.076 mg/ml pine PM for 2 hours, disruption of the monolayer by cell passaging, limited trypsin digestion, or mechanical/scratch wounding. (B) Kinetics of TRPV3 mRNA expression after cell passaging injury (left *y*-axis). The gray fill (right *y*-axis) represents cell confluence. Data were normalized to 0 hours, noninjured control cells and are presented as the mean ± S.D. from $n \geq 3$ replicates. Statistical significance was determined using one-way ANOVA with the Dunnett post-test $^{*}P < 0.05$, $^{**}P < 0.01$, $^{***}P < 0.001$, $^{****}P < 0.0001$. (C) Ca^{2+} flux assay using the TRPV3 agonist drofenine in HBEC3-KTs cultured for 24 hours postplating (~20% confluence; white) or 84 hours (100% confluent; gray). Data are presented as mean ± S.D. from $n \geq 3$ replicates, and statistical significance was determined using two-way ANOVA with the post hoc Sidak test $^{****}P < 0.0001$.

B2BV3OE cells, but the change was not statistically significant ($P > 0.05$).

Supplemental Growth Factors Partially Rescued the Scratch Wound Repair Capacity of B2BV3OE Cells. The attenuated wound repair observed for B2BV3OE, 24 hours postscratch injury, cells was partially rescued when the media was supplemented with the growth factors HB-EGF (1 ng/ml), AREG (10 ng/ml), TGFβ1 (100 ng/ml), and TGFβ2 (100 ng/ml) during a mechanical/scratch wound repair assay (Fig. 5). Images of the corresponding scratch wounds at 0 and 24 hours after scratch and supplementation of growth factors can be found in Supplemental Fig. 4.

Increased TRPV3 mRNA Expression Paralleled Increases in mRNA for EGFR Ligands after Injury, Which in Turn Stimulated TRPV3 Transcription. Increases in the expression of HB-EGF, AREG, TGFβ1, and Wnt7a mRNA occurred rapidly, and peaked ~2–4 hours after injury (Fig. 6A); EPGN, NRG1, and TGFβ2 followed the same pattern of expression (Supplemental Fig. 5). As with TRPV3, growth factor mRNA expression also decreased over time as cells restored monolayer integrity and reached 100% confluence (i.e., the 72-hour time point). Recombinant human EGFR, TGFβ1, and Fz receptor ligands were tested for their ability to regulate TRPV3 expression. Conditioned media from confluent cells was used in these experiments to avoid the effect of growth factors present in fresh media. As shown in Fig. 6B, TRPV3 mRNA increased in a dose-dependent manner because of HB-EGF, AREG, TGFβ1, and Wnt7a (as well as TGFβ2; Supplemental Fig. 5) treatment, compared with the conditioned media control.

Inhibiting EGFR, Wnt, and TGFβ Signaling Prevented Increases in TRPV3 mRNA Expression after Injury. HBEC3-KT cells were plated after passage injury in the presence of 5 μM of the following inhibitors: AG-1478

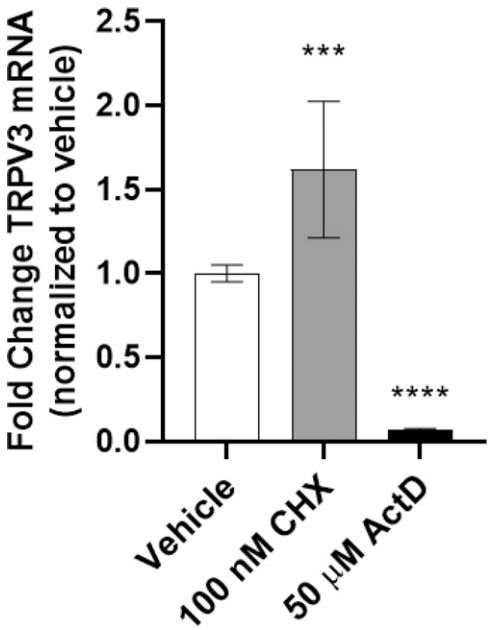

Fig. 2. Effects of transcriptional and translational inhibitors on TRPV3 mRNA expression after epithelial injury in vitro. TRPV3 expression in HBEC3-KT cells was measured 2 hours after passaging injury, with and without treatment with 50 μM ActD (a transcriptional inhibitor) or 100 nM CHX (a protein synthesis inhibitor). Statistical significance was determined using one-way ANOVA with Dunnett's post-test ***$P < 0.001$, ****$P < 0.0001$.

(EGFR/ErbB-1), AZD8931 (EGFR, ErbB2, and ErbB3), Afatinib (EGFR, ErbB2, and HER4/receptor tyrosine kinase 4), and CP-724 (ErbB2/HER2) (Fig. 7A). CP-724 treatment had minimal effect on TRPV3 transcript levels, whereas AG-1478, AZD8931, and Afatinib treatment attenuated changes in TRPV3 mRNA expression by > 60%, indicating that increases in TRPV3 expression occurred after EGFR/ErbB-1 activation, but seemingly not ErbB2, B3, or B4 activation. Although not shown, EGFR inhibition also prevented scratch wound repair by HBEC3-KT and BEAS-2B cells.

HBEC3-KT cells were also plated after passage injury in media fortified with either 10 μM SP600125 (JNK inhibitor), 10 μM PD169316 (p38 MAPK inhibitor), 20 μM CCT036477 (β-catenin inhibitor), 20 μM BMS-345541 (NF-κB inhibitor), or 5 μM TWS119 (GSK3β inhibitor). Inhibiting GSK3β, β-catenin, and p38 MAPK, as well as NF-κB, all reduced TRPV3 mRNA abundance by ~60%, indicating a key role for these molecules and the EGFR network in regulating changes in TRPV3 expression (Fig. 7, B and C). Conversely, JNK inhibition slightly increased TRPV3 expression, suggesting that JNK may negatively regulate TRPV3-increased expression after injury.

Further, Wnt and TGFβ signaling were blocked with 10 ng/ml secreted frizzled related protein 1 (prevents Wnt activation of Fzd and canonical signaling), 25 μM IWP 2 (a Porcupine inhibitor, preventing the secretion of Wnt proteins), 100 μM SB 431542 (TGFβRI inhibitor), and 150 μM ITD-1 (TGFβRII inhibitor). TRPV3 upregulation was reduced with each inhibitor, with the exception of ITD-1 (Fig. 7D).

TRPV3 Inhibition Attenuated Mouse Airway Remodeling after Subacute Oropharyngeal Exposure to Pine PM. *Trpv3* mRNA increased ~2.5-fold in the conducting airways of WSPM-treated mice ($P = 0.0214$, Fig. 8A), but not in parenchymal tissue samples (Supplemental Fig. 6) where we have also observed lower levels of TRPV3 expression in anatomically representative human cell lines (Deering-Rice et al., 2018). Representative photomicrographs (40X) of trichrome-stained C57BL/6 mouse 1st generation bronchi are shown in Fig. 8B. The epithelium of the bronchi of pine WSPM-treated mice exhibited a disorganized epithelium characterized by a stratified layer of epithelial cells stained deep red, characteristic of keratinization; a disrupted basal lamina (collagen stained blue), and a loss of ciliated cells. These morphologic anomalies

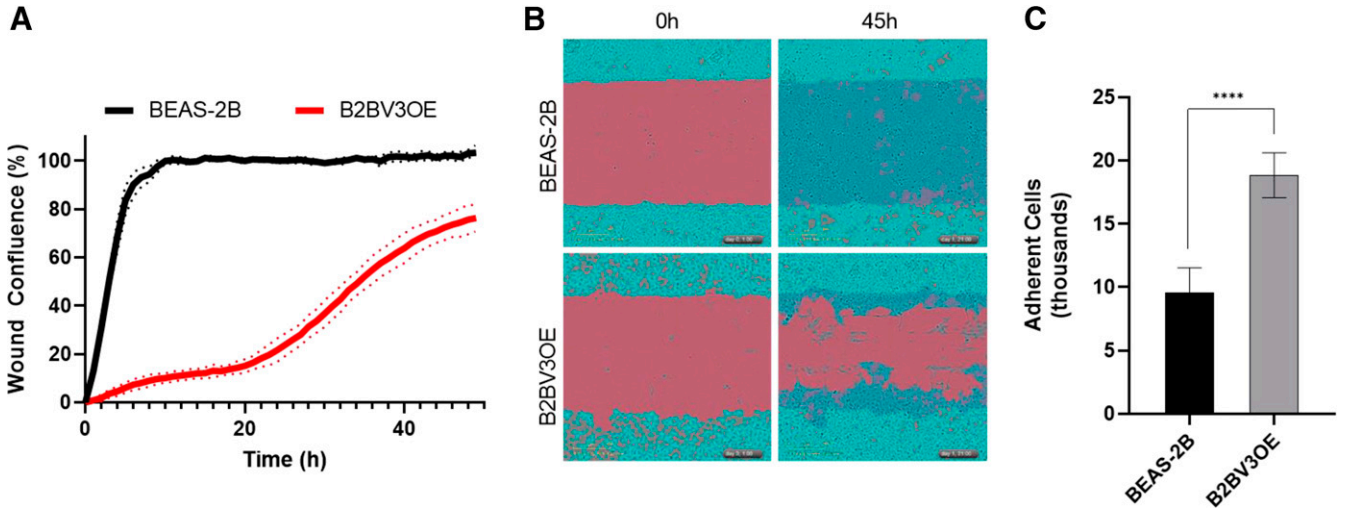

Fig. 3. Stable overexpression of TRPV3 in BEAS-2B HBECs attenuated cell migration and mechanical/scratch wound repair while increasing cell adhesion. (A) BEAS-2B cells (black line) repaired scratch wounds within 6 hours, whereas TRPV3 overexpressing BEAS-2B cells (B2BV3OE, red line) required > 48 hours. Data are shown as the mean ± S.D. (dotted lines) from $n = 4$ replicates. (B) Live-cell microscopy images (10X) of BEAS-2B and B2BV3OE cells 1 and 40 hours postscratch, with a scratch mask (red) and cell confluence mask (teal) overlaid. Videos of the entire wound repair assay are included as Supplemental Movie 1. (C) Adhesion assay comparing BEAS-2B (black) to B2BV3OE (gray) cells. Data are shown as the mean ± S.D. from $n = 8$ replicates. Statistical significance was determined using an unpaired t test. ****$P < 0.0001$.

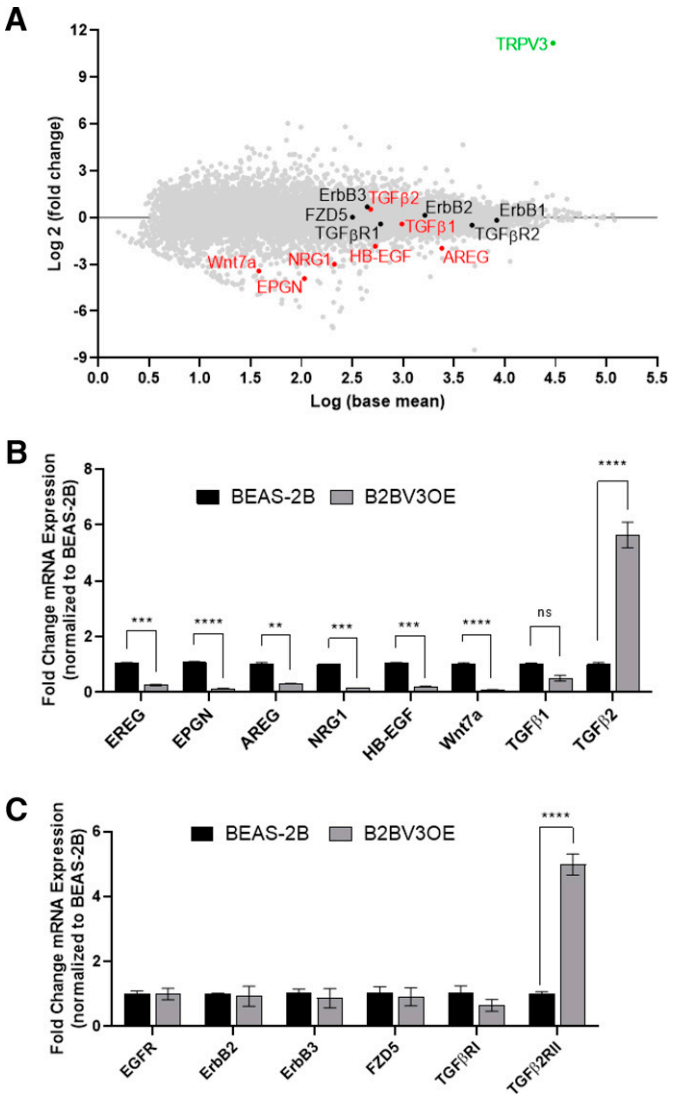

Fig. 4. Stable overexpression of TRPV3 in BEAS-2B HBECs decreased mRNA expression for multiple EGFR ligands and other canonical growth factor signaling molecules. (A) Log ratio/mean average plot of mRNA sequencing results comparing BEAS-2B and B2BV3OE cells. TRPV3 (green), the growth factors HB-EGF, AREG, NRG1, EPGN, epiregulin, TGFβ1, TGFβ2, and Wnt7a (red), and corresponding growth factor receptors (black) are highlighted. (B) Quantitative analysis of mRNA expression for epiregulin, EPGN, AREG, NRG1, HB-EGF Wnt7a, TGFβ1, and TGFβ2 in confluent B2BV3OE cells. Data were normalized to confluent BEAS-2B cells and shown as the mean ± S.D. from $n = 3$ replicates. Statistical testing was performed using two-way ANOVA with the post hoc Sidak test. *$P > 0.05$, **$P < 0.01$, ***$P < 0.001$, ****$P < 0.0001$. (C) Expression of receptors EGFR (ErbB1), ErbB2, ErbB3, FZD5, TGFβRI, and TGFβRII in confluent B2BV3OE cells compared with confluent BEAS-2B cells. Data are shown as the mean ± S.D. from $n = 3$ replicates performed using two-way ANOVA with the post hoc Sidak test. ****$P < 0.0001$.

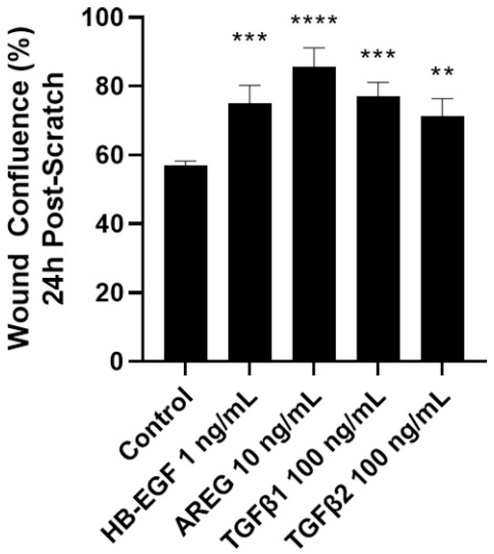

Fig. 5. Addition of downregulated growth factors to TRPV3-overexpressing cells partially rescued the repair deficiency phenotype. Supplementation of B2BV3OE cells with 1 ng/ml HB-EGF, 10 ng/ml AREG, 100 ng/ml TGFβ1, and 100 ng/ml TGFβ2 in growth media increased wound confluence during scratch wound repair compared with vehicle control B2BV3OE cells at 24 hours. Images of scratches after 24 hours are shown in Supplemental Fig. 4. Statistical significance was determined using one-way ANOVA with the Dunnett post--test. **$P < 0.01$, ***$P < 0.001$, ****$P < 0.0001$.

were consistent with the reported effects of wood smoke PM in rabbits, sheep, and humans (Thorning et al., 1982; Barrow et al., 1992; Jacob et al., 2010), and were not observed in pine PM + 007 cotreated mice or in the 007 only control group.

TRPV3 Antagonists Unexpectedly Increased TRPV3 mRNA Expression and Attenuated HBEC Migration/ Wound Repair. It was found that several TRPV3 antagonists promoted TRPV3 mRNA expression and inhibited wound repair in vitro (Fig. 9, A–F). Specifically, three structurally unique TRPV3 antagonists (i.e., 007, 008, and 2,2-diphenyltetrahydrofuran/DPTHF; Fig. 9A), which effectively block TRPV3-mediated Ca^{2+} flux (Deering-Rice et al., 2014, 2018; Nilius et al., 2014), were studied. Surprisingly, when HBEC3-KT cells were treated with the TRPV3 antagonists, TRPV3 mRNA was upregulated in excess of what occurred 2 hours postinjury alone (Fig. 9B). 008 had the strongest effect on the expression of TRPV3 ($P < 0.0001$), and all three of the antagonists attenuated monolayer wound repair (Fig. 9, C–F). Representative real-time microscopy images (10X) illustrating the extent of scratch wound repair at 48 hours are shown in Fig. 9, E and F, and time-lapse videos are included as Supplemental Movie 2 (007 and 008) and Supplemental Movie 3 (DPTHF).

TRPV3 Knockout Also Promoted TRPV3 mRNA Expression. As shown in Table 1, TRPV3KO HBEC3-KT cells expressed ~34-fold more mRNA for TRPV3 than the control cell line ($P = 0.0002$). Elevated TRPV3 mRNA expression also persisted over the time course of repair after cell passage injury. Consistent with this finding, the basal level of mRNA expression in conducting airway tissue of *Trpv3* $^{-/-}$ mice treated with saline was, on average, ~100-fold greater than in normal C57BL/6 mice ($P = 0.0073$).

Discussion

This study shows that TRPV3 is dynamically expressed by HBECs and in mouse airways after injury, and this phenomenon plays a role in wound repair and restoration of epithelial homeostasis. Additionally, TRPV3 expression and function varied over the course of the monolayer repair process, and this dynamic expression of TRPV3 is

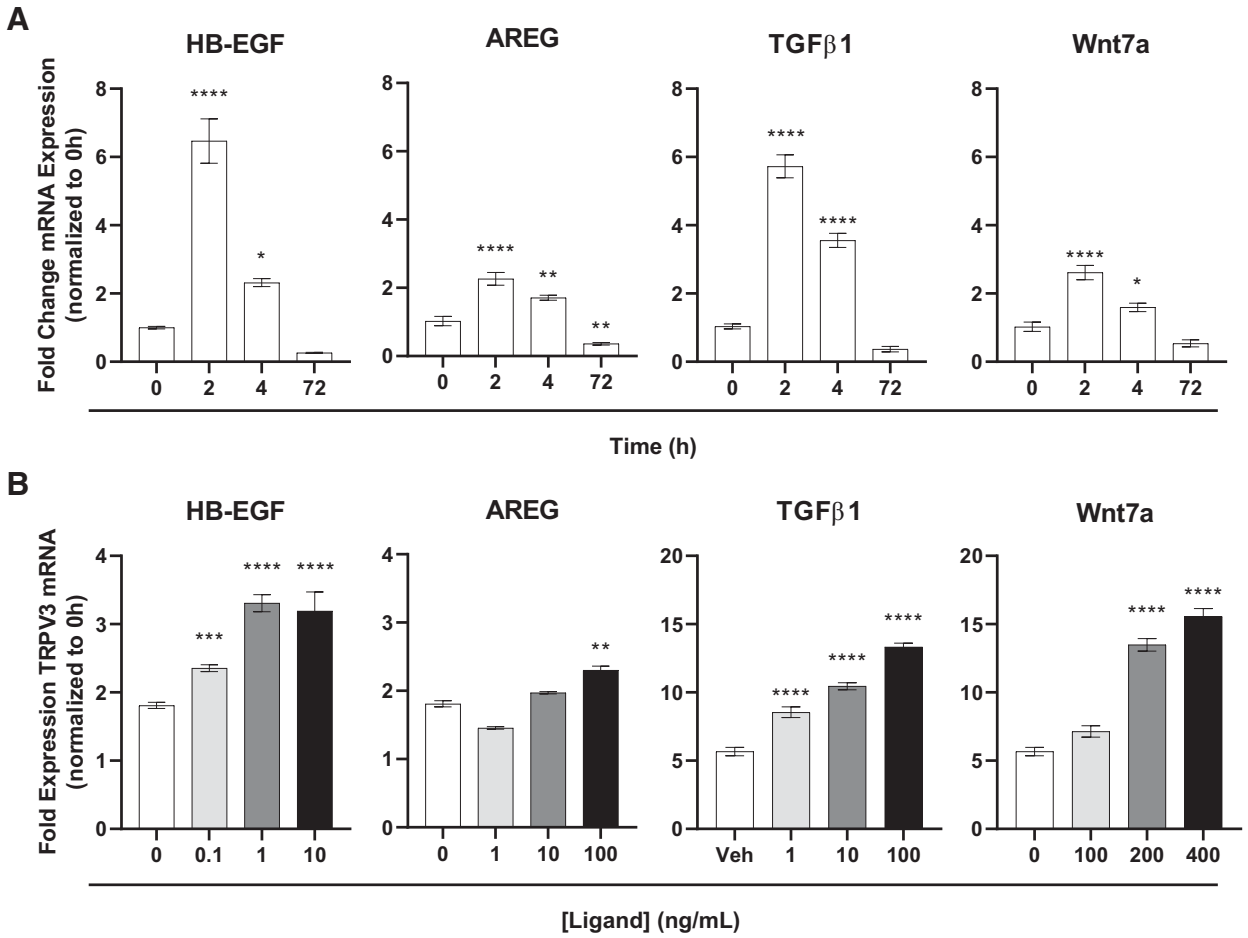

Fig. 6. Changes in EGFR, TGFβ, and Fz receptor ligand expression post–passaging injury, and TRPV3 upregulation by EGFR, TGFβ, and Fz receptor ligand supplementation. (A) Time-dependent upregulation of HB-EGF, AREG, TGFβ1, and Wnt7a mRNA in HBEC3-KT cells compared with 0 hour confluent, noninjured control cells. (B) TRPV3 mRNA expression 2 hours post–passaging injury with and without HB-EGF, AREG, TGFβ1, and Wnt7a supplementation of conditioned media. Data were normalized to 0 hour, noninjured cells and presented as mean ± S.D. from $n \geq 3$ replicates. Statistical significance was determined using one-way ANOVA with the Dunnett post-test. *$P < 0.05$, **$P < 0.01$, ***$P < 0.001$, ****$P < 0.0001$.

required to effectively coordinate repair, since inhibition of TRPV3 expression using EGFR inhibitors, stable overexpression of TRPV3, and treating cells with TRPV3 antagonists all interfered with wound repair. The rapid increase in TRPV3 expression after monolayer injury, and a decrease at later stages of repair when cells became confluent, among other results, suggests there is an optimum level of TRPV3 expression at various stages of the repair cycle, regulated via crosstalk with traditional growth factor signaling networks that drive cell motility and proliferation.

Elevated TRPV3 expression and involvement in wound repair was previously reported by Aijima et al. (2015), where it was shown that TRPV3 mRNA was upregulated 3 and 5 days post–molar tooth extraction in human oral epithelial tissue, and that *Trpv3* was necessary for healing of oral mucosa of mice. TRPV3 mRNA has also been shown to be upregulated in keratinocytes from patients with hypertrophic postburn scars, which correlated with increased TRPV3-specific Ca^{2+} flux (Kim et al., 2016). Interestingly, the TRPV3 agonist carvacrol was found to stimulate corneal epithelial cell repair at low levels, whereas higher levels became inhibitory (Yamada et al., 2010). These studies further support the concept that TRPV3 is both critical for coordinating wound repair, and that the level of TRPV3 expression and TRPV3 function is purposefully regulated by cells, to optimum levels, as a function of cell status.

Consistent with this idea, the capacity to rapidly increase TRPV3 expression in HBECs is basally present (Fig. 2). Inhibition of transcription using ActD prevented TRPV3 upregulation after injury, but inhibition of protein synthesis with CHX enhanced TRPV3 expression. These data seem to suggest the existence of a fundamental process regulating the expression of TRPV3 upon cell injury in a context-specific manner, to achieve an optimum level of expression that is presumably regulated by TRPV3 activity. Elevated TRPV3 transcript levels due to CHX treatment is also consistent with studies showing CHX treatment upregulates transcriptional activity and stabilizes mRNA, potentially through p38 MAPK and NF-κB (Hershko et al., 2004), which were found here to regulate TRPV3 mRNA expression.

Shedding of growth factors that target EGFR/ErbB and other growth factor receptors affect Ca^{2+} dynamics (Bryant et al., 2004), which regulates the injury repair

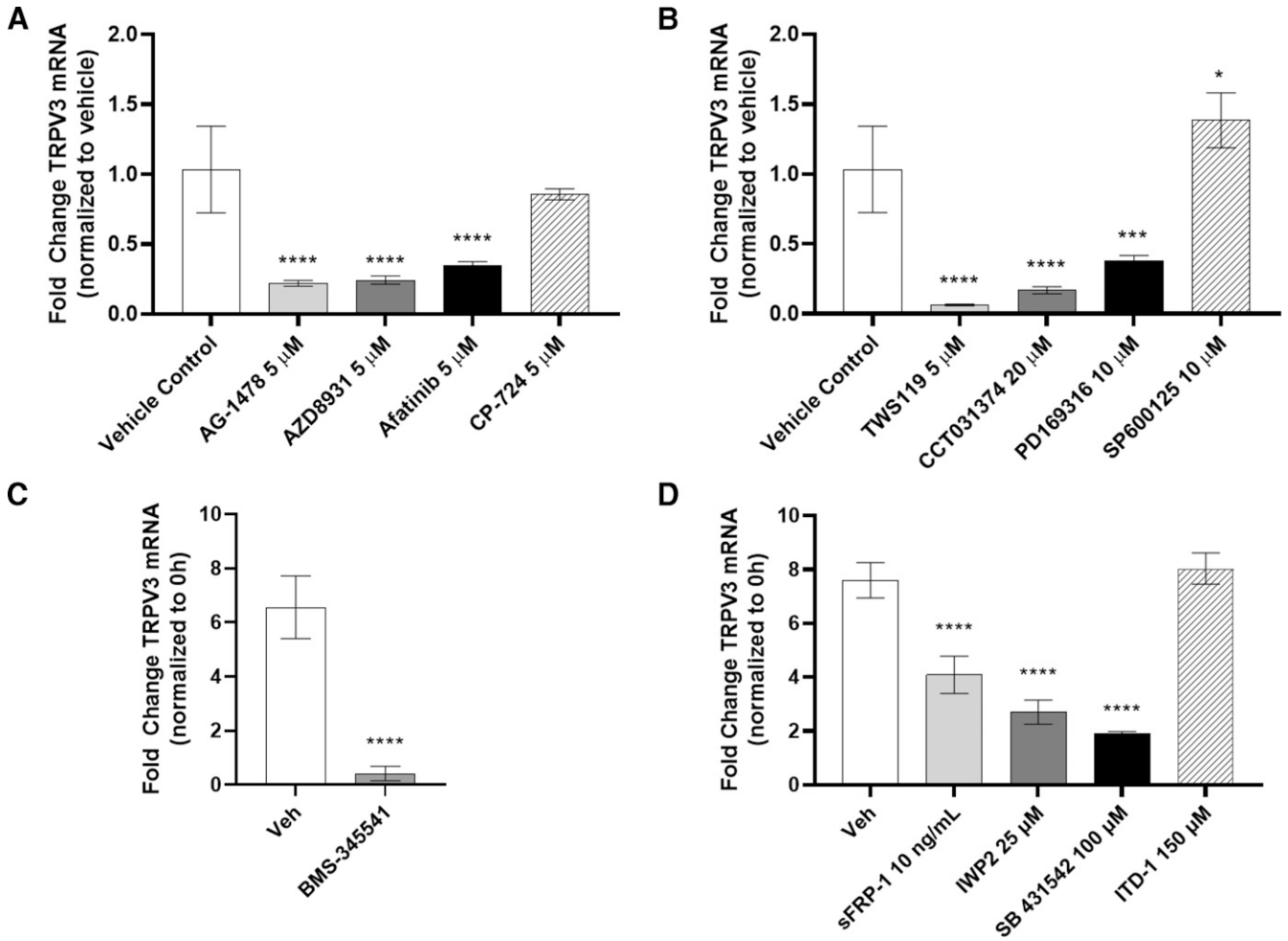

Fig. 7. Inhibition of EGFR and growth factor pathway components prevented TRPV3 mRNA upregulation after injury. (A) HBEC3-KT cells were treated with 5 μM solutions of inhibitors of multiple ErbB receptor tyrosine kinase isoforms: ErbB1 (EGFR)-specific inhibitor AG-1478, ErbB pan-inhibitors AZD8931 and Afatinib, and a selective ErbB2 (HER2) inhibitor CP-724 for 2 hours in the cell passaging injury model, followed by analysis of TRPV3 mRNA. (B) Downstream targets of EGFR activation were also inhibited, and TRPV3 expression was subsequently measured 2 hours after cell passaging injury. Inhibitors included 5 μM TWS119 (GSK3β), 20 μM CCT036477 (β-catenin), 10 μM PD169316 (p38 MAPK), and 10 μM SP600125 (JNK). (C) Inhibition of NF-κB (20 μM BMS-345541) and effects on TRPV3 mRNA 2 hours after cell passaging injury. (D) Inhibitors of Wnt7a and Fzd signaling were also used: 10 ng/ml secreted Frizzled-related protein (sFRP) and IWP 2 (Porcupine inhibitor) reduced TRPV3 upregulation after injury. Furthermore, SB 431542 (TGFβRI inhibitor) and 150 μM ITD-1 (TGFβRII inhibitor) were also tested, and SB 431542 treatment prevented TRPV3 expression as well. Values were normalized to vehicle controls and are presented as mean ± S.D. from $n \geq 3$ replicates. Statistical significance was determined using one-way ANOVA with the Dunnett post-test. ***$P < 0.001$, ****$P < 0.0001$. For Fig. 4C, an unpaired t test was used. ****$P < 0.0001$.

cycle. TRPV3-mediated Ca^{2+} flux has been linked to increased phosphorylation of EGFR in repairing oral epithelial cells, whereas knocking out *Trpv3* in mice reduced phospho-EGFR, indicating coupling between TRPV3 and EGFR signaling (Aijima et al., 2015). Further, TRPV3 activation has been linked to keratinocyte proliferation through the activation of EGFR (Wang et al., 2021). Like TRPV3, increased expression of mRNA for several EGF ligands was observed almost immediately after HBEC monolayer injury, and HB-EGF and AREG treatment promoted TRPV3 mRNA expression. Thus, it is probable that the upregulation of TRPV3 in HBECs by EGFR signaling serves to regulate Ca^{2+} dynamics within cells throughout the repair process. Furthermore, inhibition of downstream component proteins of the EGFR signaling cascade, including p38 MAPK, GSK3β, β-catenin, and NF-κB participate in the regulation of TRPV3 expression.

Wnt and TGFβ signaling also regulate epithelial repair. The expression of Wnt7a, TGFβ1, and TGFβ2 expression also increased in HBECs after injury, and all three stimulated TRPV3 mRNA expression. Like EGFR, GSK3β and β-catenin are also involved in the Wnt signaling pathway (McCubrey et al., 2014). Wnt-secreted proteins bind to Fz receptors to stabilize β-catenin, whereas translocation of β-catenin into the nucleus stimulates the transcription of Wnt target genes that facilitate development, differentiation, and cell growth (Wang et al., 2018). Additionally, TGFβ plays a role in cell repair. TGFβ isoforms bind to multiple receptors (i.e., TGFβRI, TGFβRII, and TGFβRIII) to activate TGF family receptor signaling and the expression of epithelial-to-mesenchymal transition (EMT)

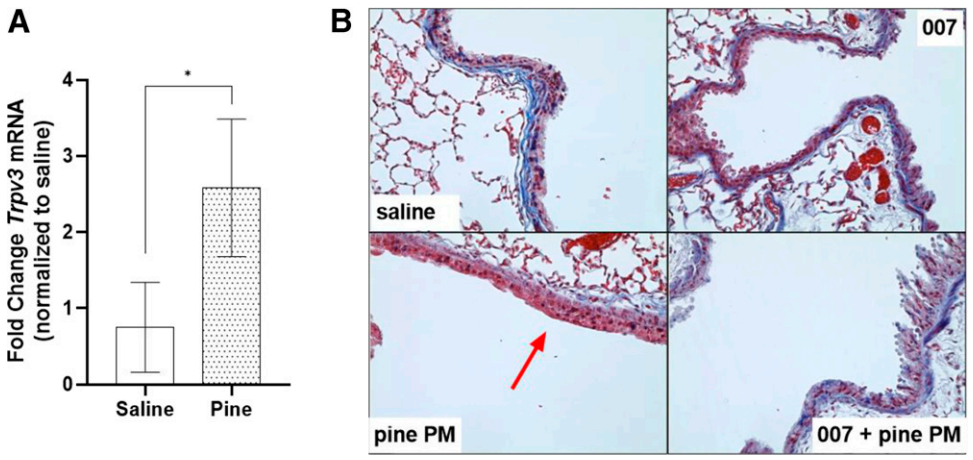

Fig. 8. Remodeling of, and *Trpv3* mRNA upregulation in the airways of mice treated with pine PM. (A) *Trpv3* mRNA expression in upper/conducting airway tissue isolated from C57BL/6 mice treated with subacute dosing of 0.5 mg/kg pine PM via OPA. Data represent the mean ± S.D. from $n \geq 3$ for each treatment, and statistical significance was determined using an unpaired t test. $^*P < 0.05$. (B) Representative photomicrographs (40X) of trichrome-stained C57BL/6 mouse 1st generation bronchial epithelium after OPA of saline or 0.5 mg/kg pine PM with and without TRPV3 antagonist (007) pre- (1 mg/kg i.p., 1 hour prior) and cotreatment (1 μM OPA). The red arrow highlights remodeled epithelium suggestive of keratinization and epithelial hyperplasia.

biomarkers, and other TGFβ-responsive genes that control differentiation and wound repair (Wendt et al., 2009). Of particular relevance are the effects of TGFβ on cell adhesion. TGFβ1 expression has been previously associated with cell migration (Giehl and Menke, 2006), whereas TGFβ2 has been linked to proliferation and adhesion (Kennedy et al., 2008). B2BV3OE cells were more adherent, whereas TRPV3KO cells were less adherent. Given that B2BV3OE cells express higher TGFβ2/TGFβRII and slightly lower TGFβ1/TGFβRI, it is likely that aberrant TGFβ signaling also contributed to the attenuated repair phenotype of B2BV3OE cells. Another interesting observation was that TGFβ2 and TGFβRII were expressed ~5.5- and 5.0-fold higher (respectively) in B2BV3OE cells. TGFβ2 supplementation has been found to arrest the cell cycle (Abraham et al., 2018) and promote adhesion (Mytilinaiou et al., 2013), whereas TGFβRII underexpression has been linked to proliferation and tumorigenesis. Conversely, TGFβRII overexpression has been associated with suppression of cell growth (Yang et al., 2017), as observed for the B2BV3OE cells. Thus, TRPV3 also appears to communicate with the Wnt/Fz and TGFβ signaling pathways to influence cell adhesion, migration, and overall repair capacity.

Overexpression of TRPV3 in BEAS-2B cells also altered the expression of several EMT genes (Supplemental Fig. 3). EMT is regulated by growth factor signaling and is a coordinated process in which cells downregulate cell adhesion and cytoskeletal proteins to become migratory mesenchymal cells. Upon monolayer repair, cells then undergo the reverse process of mesenchymal-to-epithelial transition (Xu et al., 2009). In adhesion assays, TRPV3 overexpressing cells were more adherent than BEAS-2B cells (Fig. 3C), and immunocytochemical staining for epithelial adhesion markers showed that B2BV3OE cells expressed more F-actin (an epithelial marker) compared with BEAS-2Bs (Supplemental Fig. 3). These results suggest that TRPV3 specifically interacts with growth factor signaling pathways to alter their dynamics at basal (epithelial) and in dynamic (mesenchymal) states.

The integration of TRPV3 and growth factor signaling is consistent with a prior report by Cheng et al. (2010) who demonstrated a link between TRPV3, EGFR, and TGFα signaling; proposing that EGFR signaling activates TRPV3 located on the surface of skin keratinocytes to promote the release of TGFα. These authors postulated a positive feedback loop between TRPV3 and TGFα release. This mechanism is consistent with that proposed for TGFβ, Wnt7a, and EGFR ligands in this study, with the caveat that this study implies a negative feedback mechanism for EGFR, Wnt, and TGFβ signaling, as a function of TRPV3 expression/function. This feedback is presumably maintained through the regulation of Ca^{2+} concentrations between the ER and cytosol of actively repairing cells. Although TGFα signaling was not evaluated here, transcriptomic profiling revealed negligible changes (1.14-fold) in TGFα transcripts in the B2BV3OE cells compared with BEAS-2B cells. A schematic of the cell signaling pathways that affect TRPV3 expression, and vice versa is provided by Fig. 10.

A goal of this study was to understand how variations in TRPV3 activity might affect lung injury in mice treated with WSPM. As shown, the bronchial airways of mice treated with WSPM exhibited morphologic changes including epithelial hyperplasia, which likely underlies previous findings that WSPM treatment increased airway resistance in mice, which was inhibited by the TRPV3 antagonist 007 (Deering-Rice et al., 2018). The effects of WSPM treatment are consistent with reports that low-level TRPV3 activation by agonists can promote cell growth (Yamada et al., 2010), and prior reports of the effects of wood/biomass smoke on the airway epithelium of various species (Thorning et al., 1982; Barrow et al., 1992; Jacob et al., 2010). However, in this work, we were unable to confirm a relationship between TRPV3 agonists and enhanced cell growth in vitro using HBECs or in mice, thus, we cannot rule out the possibility that TRPV3 stimulation contributed to the epithelial changes associated with WSPM exposure in mice. However, the observation that TRPV3 antagonists promote TRPV3 expression by HBECs and prevent repair, as well as the finding that *Trpv3* knockout increases *Trpv3* mRNA in mouse airways, supports the hypothesis that the protective effect of 007 on airway remodeling

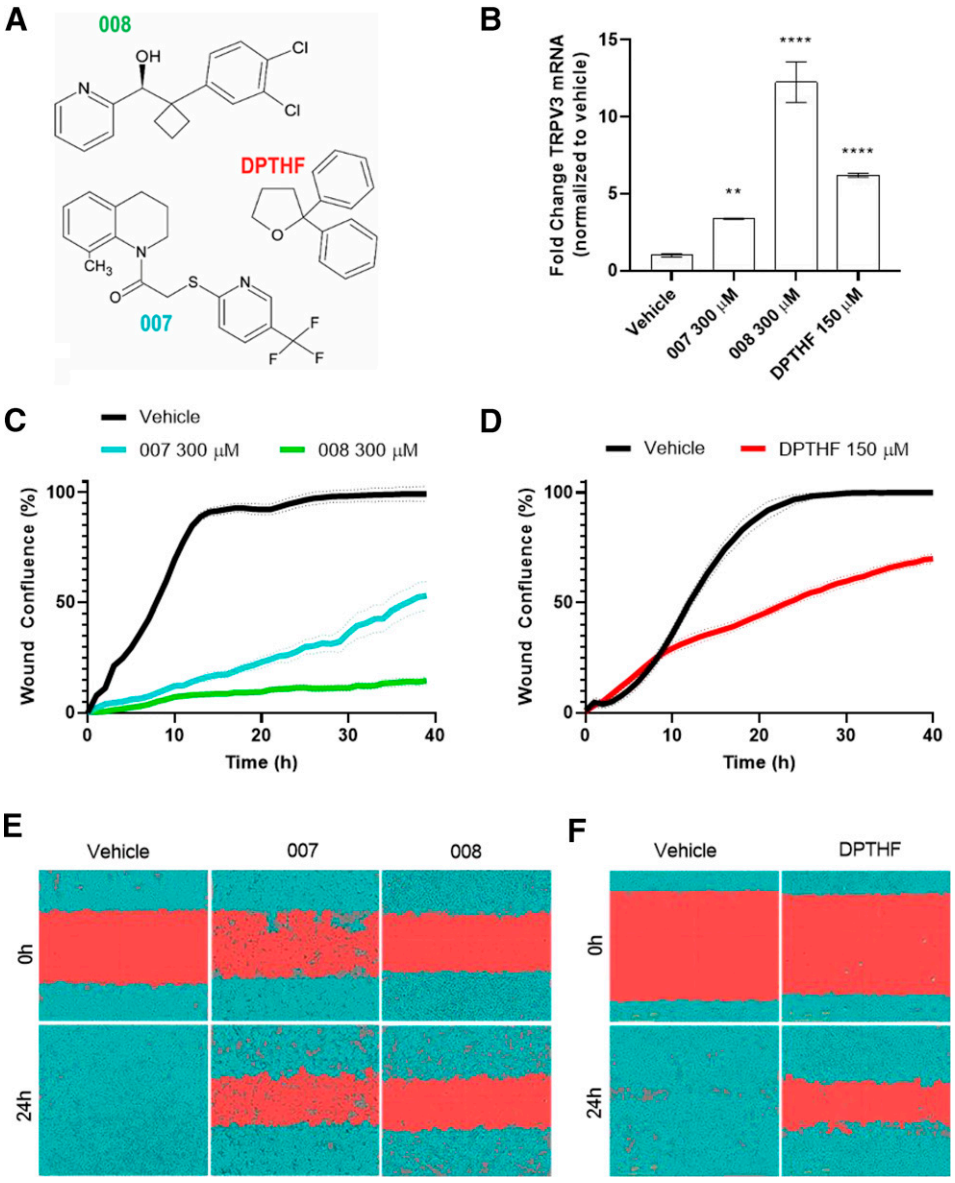

Fig. 9. Structurally unique TRPV3 antagonists increased TRPV3 mRNA expression in HBECs and slowed wound repair. (A) Chemical structures of the TRPV3 antagonists 008, 007, and DPTHF. (B) TRPV3 mRNA expression was increased in confluent HBEC3-KT cells after 2 hours treatment with multiple TRPV3 antagonists. Data were normalized to vehicle controls and are presented as the mean ± S.D. from $n \geq 3$ replicates. Statistical significance was determined using one-way ANOVA with the Dunnett post-test. $^{**}P < 0.01$, $^{****}P < 0.0001$. Scratch wound repair of HBEC3-KT cells treated with (C) 007 (teal line) or 008 (green line) and (D) DPTHF (red line) compared with untreated controls (black lines). Growth curves are shown as the mean ± S.D. (dotted line) from $n = 3$ replicates. Live-cell microscopy images (10X) of vehicle versus (E) 300 μM 008 treated cells, and (F) DPTHF treated cells, 0 and 48 hours postscratch. A scratch mask (red) and confluence mask (teal) are overlaid. Videos of the antagonist effect on wound repair are included as Supplemental Movie 2 (008 and 007) and Supplemental Movie 3 (DPTHF).

may be the result of increased TRPV3 expression, mimicking the effects of TRPV3 overexpression in HBECs, as TRPV3 knockout in HBEC3-KT cells does not prevent epithelial repair. However, this paradigm requires further study.

To summarize, TRPV3 appears to be crucial in regulating airway epithelial cell repair, and the findings related to the alterations in TRPV3 expression and activity caused by various biochemical and pharmacological manipulations could have broad significance in the development of therapeutics and furthering our understanding of the pathogenesis of selected respiratory diseases.

TABLE 1

Elevated TRPV3 mRNA expression in TRPV3KO HBEC3-KT and conducting airway tissue of *Trpv3*−/− mice.

TRPV3 mRNA expression in HBECs is normalized to the HBEC3-KT control and presented as the mean ± S.D. from $n = 4$ replicates. Statistical significance was determined using an unpaired t test ($^{***}P < 0.001$). *Trpv3* mRNA expression in mouse lung tissue is normalized to the C57BL/6 control and presented as the mean ± S.D. from $n \geq 4$ replicates. Statistical significance was determined using an unpaired t test ($^{**}P < 0.01$).

Model Identity	TRPV3 mRNA (Fold Control)
HBEC-3KT cells	1.00 ± 0.03
TRPV3KO HBEC3-KT cells	34 ± 7***
C57BL/6 mice	1.2 ± 0.8
Trpv3$^{-/-}$ C57BL/6 mice	110 ± 54**

HBEC-3KT, normal human bronchial epithelial cells immortalized with CDK4 and hTERT.

Authorship Contributions

Participated in research design: Burrell, Nguyen, Deering-Rice, Memon, Lamb, Reilly.

Conducted experiments: Burrell, Nguyen, Deering-Rice, Memon, Almestica-Roberts, Rapp, Serna, Lamb, Reilly.

Performed data analysis: Burrell, Nguyen, Deering-Rice, Memon, Almestica-Roberts, Rapp, Reilly.

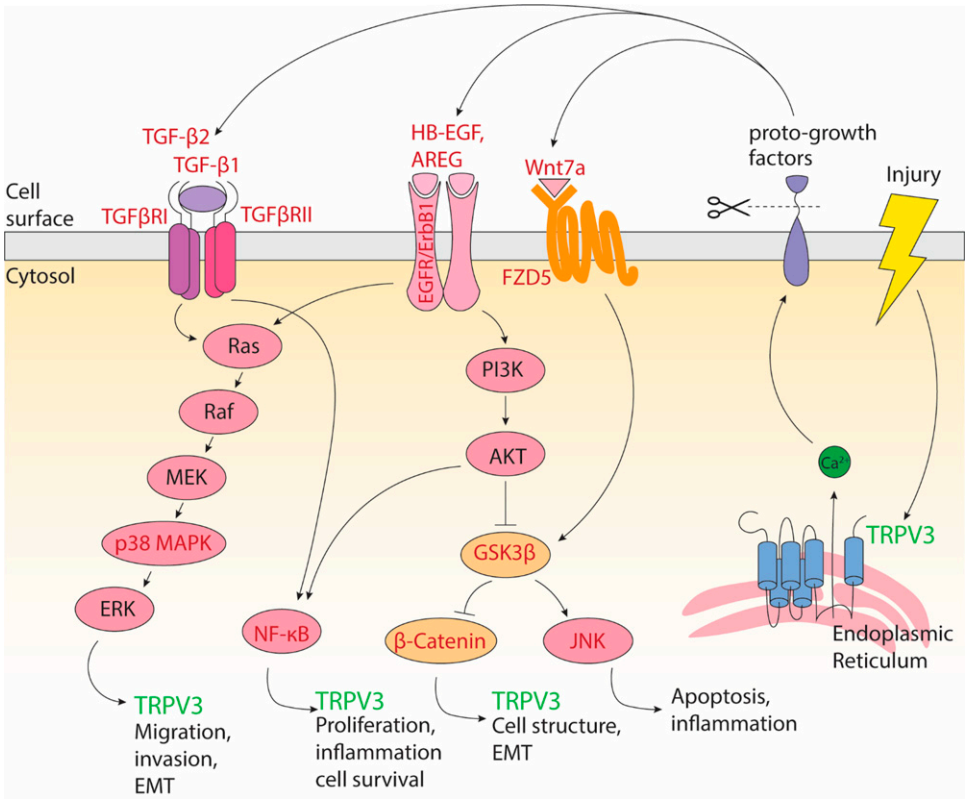

Fig. 10. Summary schematic of cell signaling pathways that influence, and in turn are influenced by, TRPV3 activity and expression within lung epithelial cells after simulated epithelial injury. Components tested in this study are highlighted as red text. EGFR ligands, TGFβ, and Wnt signaling factors activate signaling cascades including p38 MAPK, NF-κB, GSK3β, and β-catenin to affect TRPV3 expression after injury. It is further suggested that TRPV3 expression and activity in turn affect growth factor expression and shedding to slow repair and to restore proper epithelial homeostasis after injury repair. Other components related to the signaling cascades shown include Ras (a family of small GTPases), Raf (family of kinases), PI3K (Phosphoinositide 3-kinase), MEK (Mitogen-activated protein kinase kinase) and ERK (Extracellular signal-regulated kinase).

Wrote or contributed to writing of the manuscript: Burrell, Nguyen, Deering-Rice, Memon, Almestica-Roberts, Reilly.

References

Abraham CG, Ludwig MP, Andrysik Z, Pandey A, Joshi M, Galbraith MD, Sullivan KD, and Espinosa JM (2018) ΔNp63α suppresses TGFB2 expression and RHOA activity to drive cell proliferation in squamous cell carcinomas. *Cell Rep* **24**:3224–3236.

Aijima R, Wang B, Takao T, Mihara H, Kashio M, Ohsaki Y, Zhang J-Q, Mizuno A, Suzuki M, Yamashita Y, et al. (2015) The thermosensitive TRPV3 channel contributes to rapid wound healing in oral epithelia. *FASEB J* **29**:182–192 Federation of American Societies for Experimental Biology.

Barrow RE, Wang C-Z, Cox RA, and Evans MJ (1992) Cellular sequence of tracheal repair in sheep after smoke inhalation injury. *Lung* **170**:331–338.

Borbíró I, Lisztes E, Tóth BI, Czifra G, Oláh A, Szöllosi AG, Szentandrássy N, Nánási PP, Péter Z, Paus R, et al. (2011) Activation of transient receptor potential vanilloid-3 inhibits human hair growth. *J Invest Dermatol* **131**:1605–1614.

Bryant JA, Finn RS, Slamon DJ, Cloughesy TF, and Charles AC (2004) EGF activates intracellular and intercellular calcium signaling by distinct pathways in tumor cells. *Cancer Biol Ther* **3**:1243–1249 Taylor & Francis.

Cheng X, Jin J, Hu L, Shen D, Dong XP, Samie MA, Knoff J, Eisinger B, Liu ML, Huang SM, et al. (2010) TRP channel regulates EGFR signaling in hair morphogenesis and skin barrier formation. *Cell* **141**:331–343.

Cordeiro JV and Jacinto A (2013) The role of transcription-independent damage signals in the initiation of epithelial wound healing. *Nat Rev Mol Cell Biol* **14**:249–262.

Crosby LM and Waters CM (2010) Epithelial repair mechanisms in the lung. *Am J Physiol Lung Cell Mol Physiol* **298**:L715–L731 American Physiological Society.20363851

Deering-Rice CE, Memon T, Lu Z, Romero EG, Cox J, Taylor-Clark T, Veranth JM, and Reilly CA (2019) Differential activation of TRPA1 by diesel exhaust particles: Relationships between chemical composition, potency, and lung toxicity. *Chem Res Toxicol* **32**:1040–1050 American Chemical Society.

Deering-Rice CE, Mitchell VK, Romero EG, Abdel Aziz MH, Ryskamp DA, Križaj D, Gopal VR, and Reilly CA (2014) Drofenine: a 2-APB analog with improved selectivity for human TRPV3. *Pharmacol Res Perspect* **2**:e00062 John Wiley & Sons, Ltd.

Deering-Rice CE, Nguyen N, Lu Z, Cox JE, Shapiro D, Romero EG, Mitchell VK, Burrell KL, Veranth JM, and Reilly CA (2018) Activation of TRPV3 by wood smoke particles and roles in pneumotoxicity. *Chem Res Toxicol* **31**:291–301 American Chemical Society.

Deering-Rice CE, Romero EG, Shapiro D, Hughen RW, Light AR, Yost GS, Veranth JM, and Reilly CA (2011) Electrophilic components of diesel exhaust particles (DEP) activate transient receptor potential ankyrin-1 (TRPA1): a probable mechanism of acute pulmonary toxicity for DEP. *Chem Res Toxicol* **24**:950–959 American Chemical Society.

Delgado O, Kaisani AA, Spinola M, Xie X-J, Batten KG, Minna JD, Wright WE, and Shay JW (2011) Multipotent capacity of immortalized human bronchial epithelial cells. *PLoS One* **6**:e22023 Public Library of Science.

Edgar R, Domrachev M, and Lash AE (2002) Gene expression omnibus: NCBI gene expression and hybridization array data repository. *Nucleic Acids Res* **30**:207–210.

Fabian A, Fortmann T, Dieterich P, Riethmüller C, Schön P, Mally S, Nilius B, and Schwab A (2008) TRPC1 channels regulate directionality of migrating cells. *Pflugers Arch* **457**:475–484.

Fiorio Pla A, Ong HL, Cheng KT, Brossa A, Bussolati B, Lockwich T, Paria B, Munaron L, and Ambudkar IS (2012) TRPV4 mediates tumor-derived endothelial cell migration via arachidonic acid-activated actin remodeling. *Oncogene* **31**:200–212.

Ghio AJ, Soukup JM, Case M, Dailey LA, Richards J, Berntsen J, Devlin RB, Stone S, and Rappold A (2012) Exposure to wood smoke particles produces inflammation in healthy volunteers. *Occup Environ Med* **69**:170–175.

Giehl K and Menke A (2006) Moving on: Molecular mechanisms in TGFβ-induced epithelial cell migration. *Signal Transduct* **6**:355–364 John Wiley & Sons, Ltd.

Gomtsyan A, Schmidt RG, Bayburt EK, Gfesser GA, Voight EA, Daanen JF, Schmidt DL, Cowart MD, Liu H, Altenbach RJ, et al. (2016) Synthesis and pharmacology of (pyridin-2-yl)methanol derivatives as novel and selective transient receptor potential vanilloid 3 antagonists. *J Med Chem* **59**:4926–4947 American Chemical Society.

Hershko DD, Robb BW, Wray CJ, Luo GJ, and Hasselgren P-O (2004) Superinduction of IL-6 by cycloheximide is associated with mRNA stabilization and sustained activation of p38 map kinase and NF-kappaB in cultured caco-2 cells. *J Cell Biochem* **91**:951–961 John Wiley & Sons, Ltd.

Jacob S, Kraft R, Zhu Y, Jacob RK, Herndon DN, Traber DL, Hawkins HK, and Cox RA (2010) Acute secretory cell toxicity and epithelial exfoliation after smoke inhalation injury in sheep: an electron and light microscopic study. *Toxicol Mech Methods* **20**:504–509 Taylor & Francis.

Kennedy L, Shi-Wen X, Carter DE, Abraham DJ, and Leask A (2008) Fibroblast adhesion results in the induction of a matrix remodeling gene expression program. *Matrix Biol* **27**:274–281.

Kim HO, Cho YS, Park SY, Kwak IS, Choi MG, Chung BY, Park CW, and Lee JY (2016) Increased activity of TRPV3 in keratinocytes in hypertrophic burn scars with postburn pruritus. *Wound Repair Regen* **24**:841–850 John Wiley & Sons. Ltd

Laumbach RJ and Kipen HM (2012) Respiratory health effects of air pollution: update on biomass smoke and traffic pollution. *J Allergy Clin Immunol* **129**:3–11, quiz 12–13.

Lin Z, Chen Q, Lee M, Cao X, Zhang J, Ma D, Chen L, Hu X, Wang H, Wang X, et al. (2012) Exome sequencing reveals mutations in TRPV3 as a cause of Olmsted syndrome. *Am J Hum Genet* **90**:558–564.

Liu Sha, Zhou Y, Liu Suixin, Chen X, Zou W, Zhao D, Li X, Pu J, Huang L, Chen J, Li B, Liu Shiliang, and Ran P (2017) Association between exposure to ambient particulate matter and chronic obstructive pulmonary disease: results from a cross-sectional study in China. *Thorax* **72**:788–795.

Martin E, Dahan D, Cardouat G, Gillibert-Duplantier J, Marthan R, Savineau J-P, and Ducret T (2012) Involvement of TRPV1 and TRPV4 channels in migration of rat pulmonary arterial smooth muscle cells. *Pflugers Arch* **464**:261–272.

McCubrey JA, Steelman LS, Bertrand FE, Davis NM, Sokolosky M, Abrams SL, Montalto G, D'Assoro AB, Libra M, Nicoletti F, et al. (2014) GSK-3 as potential target for therapeutic intervention in cancer. *Oncotarget* **5**:2881–2911 Impact Journals LLC.

McLean WHI and Irvine AD (2007) Disorders of keratinisation: from rare to common genetic diseases of skin and other epithelial tissues. *Ulster Med J* **76**:72–82 The Ulster Medical Society.

Memon TA, Nguyen ND, Burrell KL, Scott AF, Almestica-Roberts M, Rapp E, Deering-Rice CE, and Reilly CA (2020) Wood smoke particles stimulate MUC5AC overproduction by human bronchial epithelial cells through TRPA1 and EGFR signaling. *Toxicol Sci* **174**:278–290.

Middelbeek J, Visser D, Henneman L, Kamermans A, Kuipers AJ, Hoogerbrugge PM, Jalink K, and van Leeuwen FN (2015) TRPM7 maintains progenitor-like features of neuroblastoma cells: implications for metastasis formation. *Oncotarget* **6**:8760–8776 Impact Journals LLC.

Monet M, Gkika D, Lehen'kyi V, Pourtier A, Vanden Abeele F, Bidaux G, Juvin V, Rassendren F, Humez S, and Prevarsakaya N (2009) Lysophospholipids stimulate prostate cancer cell migration via TRPV2 channel activation. *Biochim Biophys Acta* **1793**:528–539.

Mytilinaiou M, Bano A, Nikitovic D, Berdiaki A, Voudouri K, Kalogeraki A, Karamanos NK, and Tzanakakis GN (2013) Syndecan-2 is a key regulator of transforming growth factor beta 2/Smad2-mediated adhesion in fibrosarcoma cells. *IUBMB Life* **65**:134–143 England.

Nguyen ND, Memon TA, Burrell KL, Almestica-Roberts M, Rapp E, Sun L, Scott AF, Rower JE, Deering-Rice CE, and Reilly CA (2020) Transient receptor potential ankyrin-1 and vanilloid-3 differentially regulate endoplasmic reticulum stress and cytotoxicity in human lung epithelial cells after pneumotoxic wood smoke particle exposure. *Mol Pharmacol* **98**:586–597.

Nilius B, Bíró T, and Owsianik G (2014) TRPV3: time to decipher a poorly understood family member! *J Physiol* **592**:295–304 John Wiley & Sons. Ltd

Olloquequi J and Silva O R (2016) Biomass smoke as a risk factor for chronic obstructive pulmonary disease: effects on innate immunity. *Innate Immun* **22**:373–381 SAGE Publications Ltd STM.

Reid CE, Brauer M, Johnston FH, Jerrett M, Balmes JR, and Elliott CT (2016) Critical review of health impacts of wildfire smoke exposure. *Environ Health Perspect* **124**:1334–1343 Environmental Health Perspectives.

Shapiro D, Deering-Rice CE, Romero EG, Hughen RW, Light AR, Veranth JM, and Reilly CA (2013) Activation of transient receptor potential ankyrin-1 (TRPA1) in lung cells by wood smoke particulate material. *Chem Res Toxicol* **26**:750–758 American Chemical Society.

Swiston JR, Davidson W, Attridge S, Li GT, Brauer M, and van Eeden SF (2008) Wood smoke exposure induces a pulmonary and systemic inflammatory response in firefighters. *Eur Respir J* **32**:129–138.

Thorning DR, Howard ML, Hudson LD, and Schumacher RL (1982) Pulmonary responses to smoke inhalation: morphologic changes in rabbits exposed to pine wood smoke. *Hum Pathol* **13**:355–364.

Wang Y, Li H, Xue C, Chen H, Xue Y, Zhao F, Zhu MX, and Cao Z (2021) TRPV3 enhances skin keratinocyte proliferation through EGFR-dependent signaling pathways. *Cell Biol Toxicol* **37**:313–330.

Wang Z, Li R, He Y, and Huang S (2018) Effects of secreted frizzled-related protein 1 on proliferation, migration, invasion, and apoptosis of colorectal cancer cells. *Cancer Cell Int* **18**:48.

Wendt MK, Allington TM, and Schiemann WP (2009) Mechanisms of the epithelial-mesenchymal transition by TGF-beta. *Future Oncol* **5**:1145–1168.

Wondergem R and Bartley JW (2009) Menthol increases human glioblastoma intracellular Ca2+, BK channel activity and cell migration. *J Biomed Sci* **16**:90 BioMed Central.

Xu J, Lamouille S, and Derynck R (2009) TGF-β-induced epithelial to mesenchymal transition. *Cell Res* **19**:156–172.

Yamada T, Ueda T, Ugawa S, Ishida Y, Imayasu M, Koyama S, and Shimada S (2010) Functional expression of transient receptor potential vanilloid 3 (TRPV3) in corneal epithelial cells: involvement in thermosensation and wound healing. *Exp Eye Res* **90**:121–129.

Yang H, Zhang H, Zhong Y, Wang Q, Yang L, Kang H, Gao X, Yu H, Xie C, Zhou F, et al. (2017) Concomitant underexpression of TGFBR2 and overexpression of hTERT are associated with poor prognosis in cervical cancer. *Sci Rep* **7**:41670.

Zemans RL, McClendon J, Aschner Y, Briones N, Young SK, Lau LF, Kahn M, and Downey GP (2013) Role of β-catenin-regulated CCN matricellular proteins in epithelial repair after inflammatory lung injury. *Am J Physiol Lung Cell Mol Physiol* **304**:L415–L427 American Physiological Society.

Corresponding Author: Dr. Christopher A. Reilly, Department of Pharmacology and Toxicology, Center for Human Toxicology, University of Utah, 30 S. 2000 E., Room 201 Skaggs Hall, Salt Lake City, UT 84112. E-mail: Chris.Reilly@pharm.utah.edu

Supplementary Information:

Title: Dynamic Expression of TRPV3 and Integrated Signaling with Growth Factor Pathways During Lung Epithelial Wound Repair Following Wood Smoke Particle and Other Forms of Lung Cell Injury

Journal Title: Molecular Pharmacology

Authors: Katherine L. Burrell, Nam D. Nguyen, Cassandra E. Deering-Rice, Tosifa A. Memon, Marysol Almestica-Roberts, Emmanuel Rapp, Samantha N. Serna, John G. Lamb, and Christopher A. Reilly

Affiliations: (KLB, NDN, CEDR, TAM, MAR, ER, SNS, JGL, CAR) Department of Pharmacology and Toxicology, Center for Human Toxicology, University of Utah, 30 S 2000 E, Room 201 Skaggs Hall, Salt Lake City, Utah 84112, United States

Manuscript Number: MOLPHARM-AR-2021-000280

Methods:

Western blotting: HBEC3-KT cells were plated into T-25 flasks and harvested at various time points. BEAS2-B TRPV3OE cells were used as a positive control and harvested at 100% confluence. Cells were lysed using RIPA buffer (ThermoFisher) supplemented with 6M urea and fortified with Halt™ Phosphatase and Protease Inhibitor Cocktail (ThermoFisher). Total protein yields were determined the BCA protein assay (ThermoFisher) and 30 μg of protein/sample was loaded into 4-12% Bolt Bis-Tris 12-well gels (ThermoFisher). TRPV3 protein expression was measured using a 1:500 dilution of a mouse anti-TRPV3 primary antibody (75-043, NeuroMab, Davis CA), and band intensity was quantified using ImageJ software.

Immunocytochemistry: BEAS-2B and BEAS-2B TRPV3OE cells were plated on 8-well chamber slides, which were coated with LHC basal medium fortified with collagen (30 μg/mL), fibronectin (10 μg/mL), and bovine serum albumin fraction V (100 μg/mL). Cells were incubated for 2 hours to allow adhesion and then fixed with 4% paraformaldehyde and permeabilized with 0.2% Triton X-100. Blocking was done with 10% normal goat serum for 1h at room temperature (~22°C). To probe for TRPV3, cells were incubated with a mouse monoclonal primary antibody for TRPV3 (1:200; 73-043; Neuromab; Davis, CA) overnight at 4ºC, followed by incubation with a goat-anti-mouse secondary antibody conjugated with AlexaFluor594 (1:1000, A-11032, Invitrogen; Carlsbad, CA). After incubation with the antibodies, F-acting (phalloidin) was stained with ActinGreen conjugated with AlexaFluor488 (R37110, Invitrogen, Carlsbad, CA) and cell nuclei were stained with Hoechst 33342. Cells were then fixed with 4% paraformaldehyde and imaged.

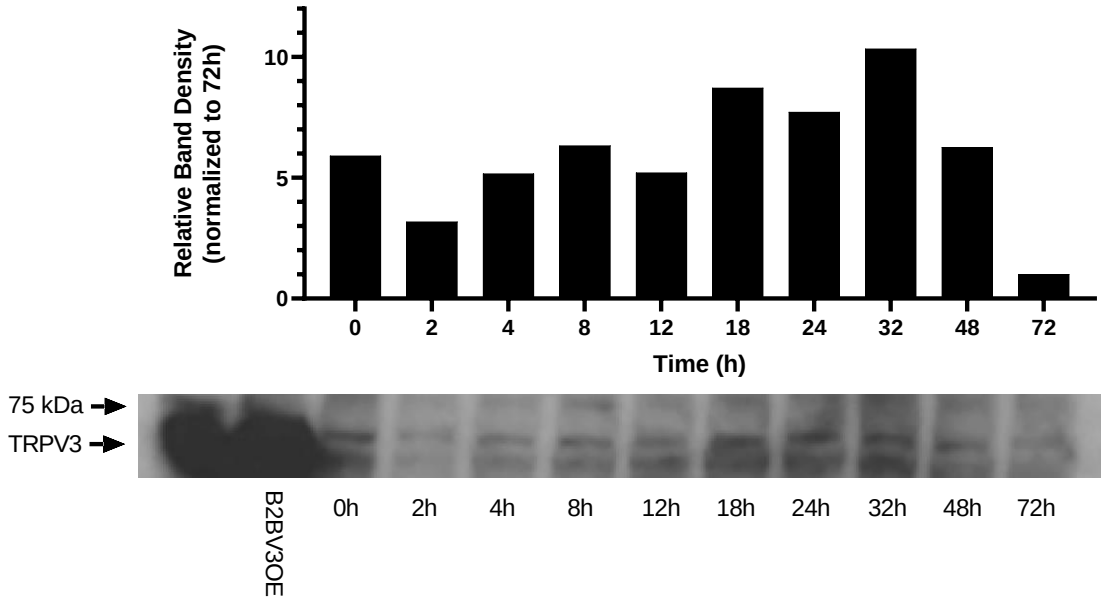

Supplemental Figure 1. Western blot analysis of TRPV3 protein (70 kDa) in HBEC3-KT cells versus time after cell passaging injury. Lysate from B2BV3OE cells was used as a positive control.

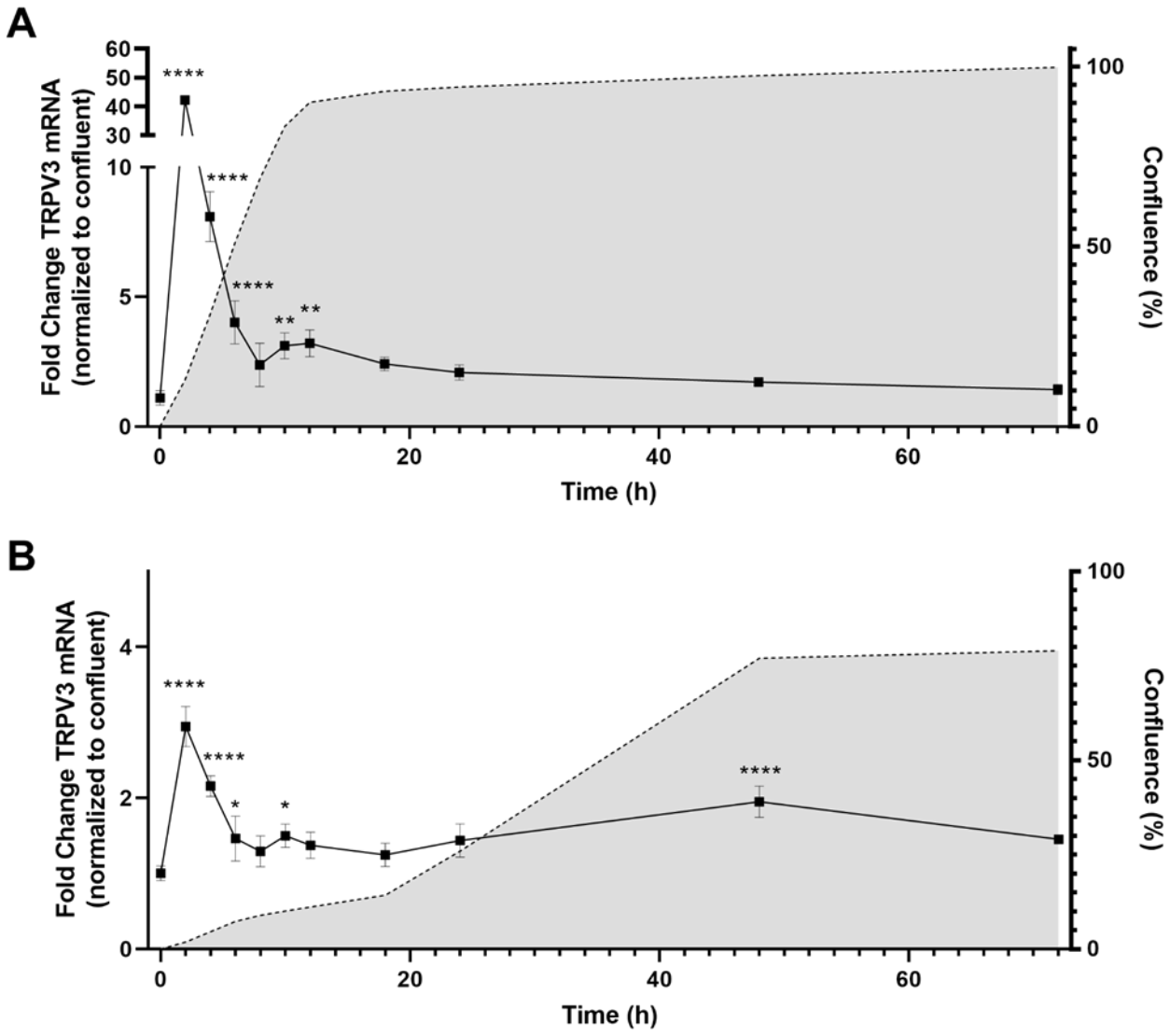

Supplemental Figure 2. TRPV3 expression over time in **A)** BEAS-2B and **B)** B2BV3OE cells. Data were normalized to 0h confluent control cells and are represented as the mean ± SD from *n* = 3 replicates. The grey fill (right y-axis) represents cell confluence. Statistical significance was determined using one-way ANOVA with the Dunnett post-test. **p* < 0.05, ***p* < 0.01, ****p* < 0.001, *****p* < 0.0001.

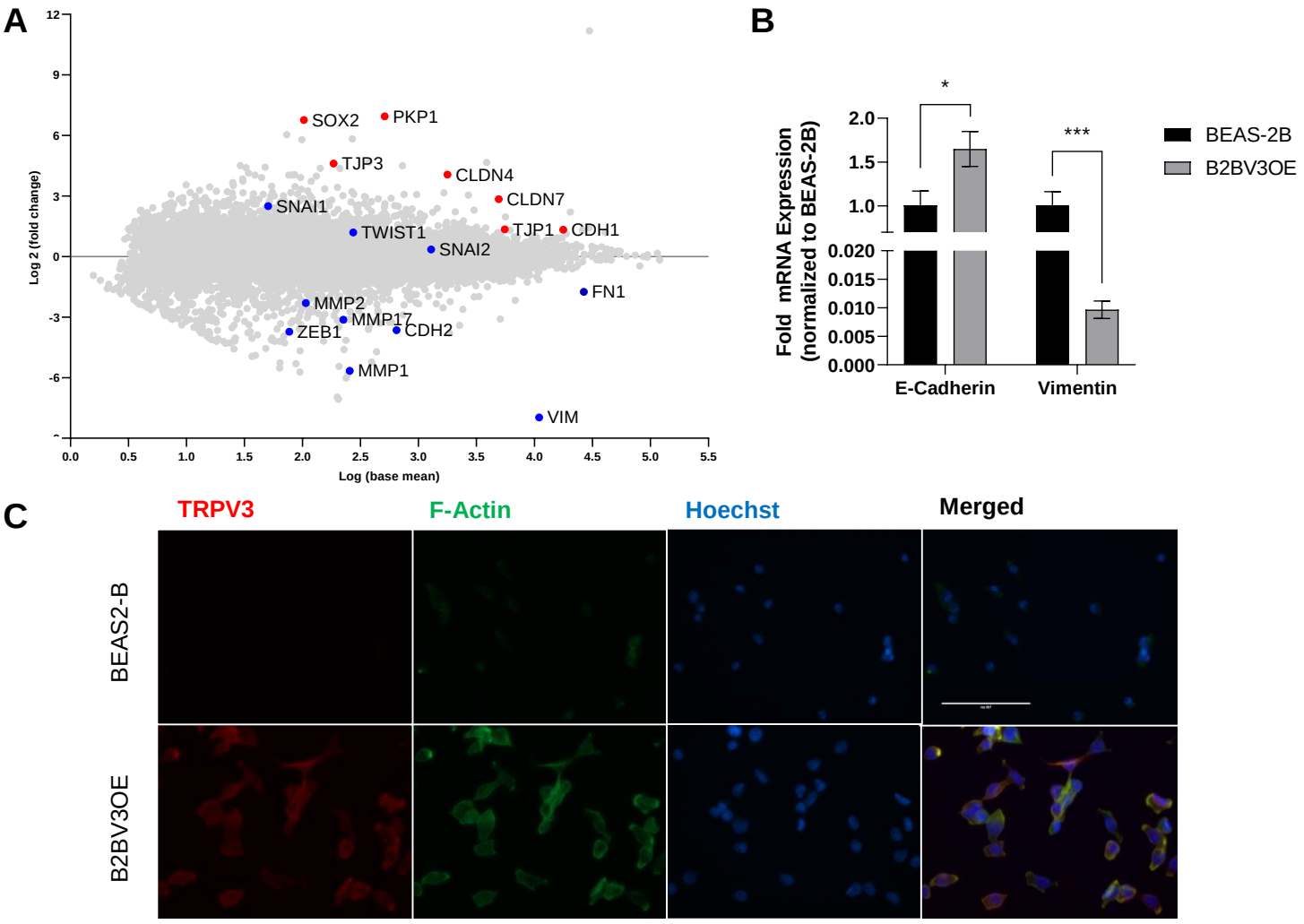

Supplemental Figure 3. Comparative expression of mRNA and protein for several epithelial and mesenchymal markers in BEAS2B and B2BV3OE cells. **A)** MA plot of RNAseq data illustrating differences in epithelial (red) and mesenchymal (blue) markers. **B)** Quantitative PCR results comparing vimentin and E-cadherin mRNA expression. **C)** Immunocytochemical analysis of TRPV3 (red) and F-Actin (green) in BEAS-2B and B2BV3OE cells.

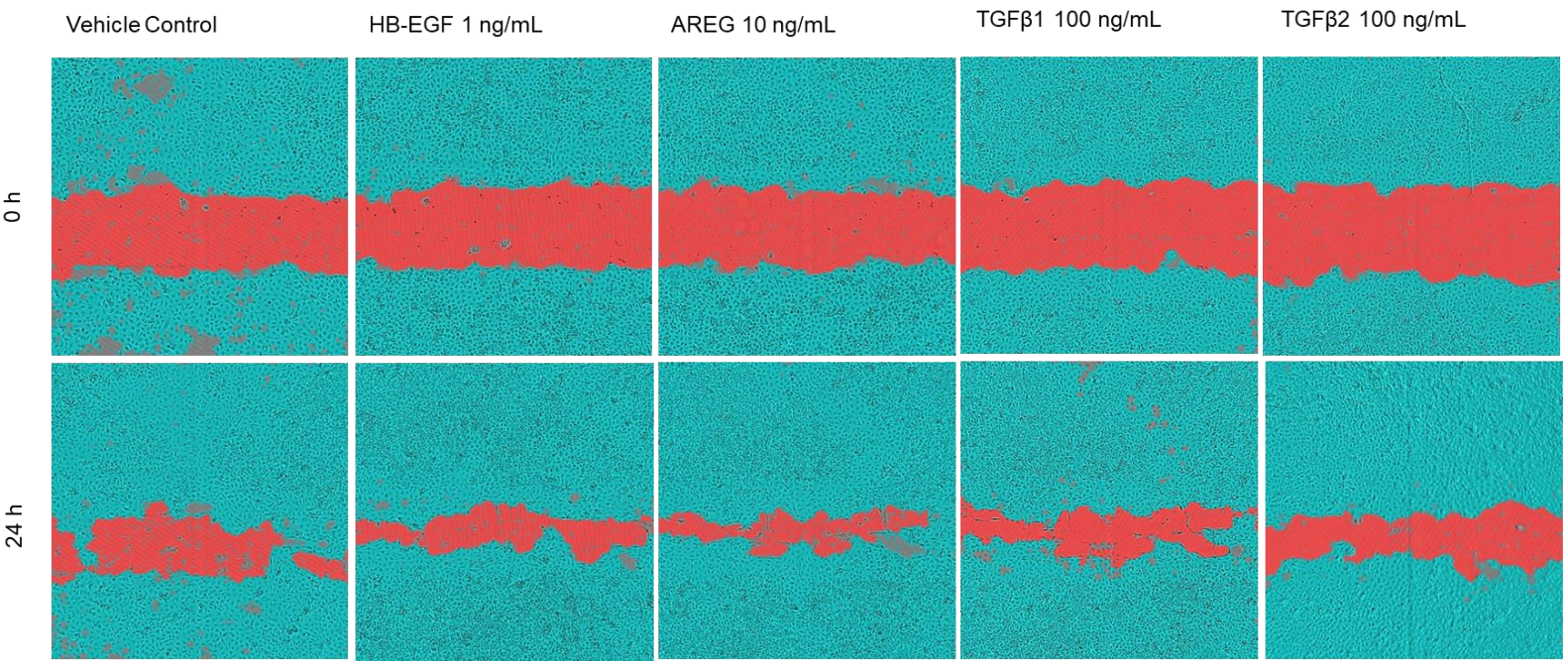

Supplemental Figure 4. Scratch wound repair images of B2BV3OE cells at 0 and 24h after injury when cultured in conditioned media with or without 1 ng/mL recombinant HB-EGF, 10 ng/mL AREG, 100 ng/mL TGFβ1 or 100 ng/mL TGFβ2.

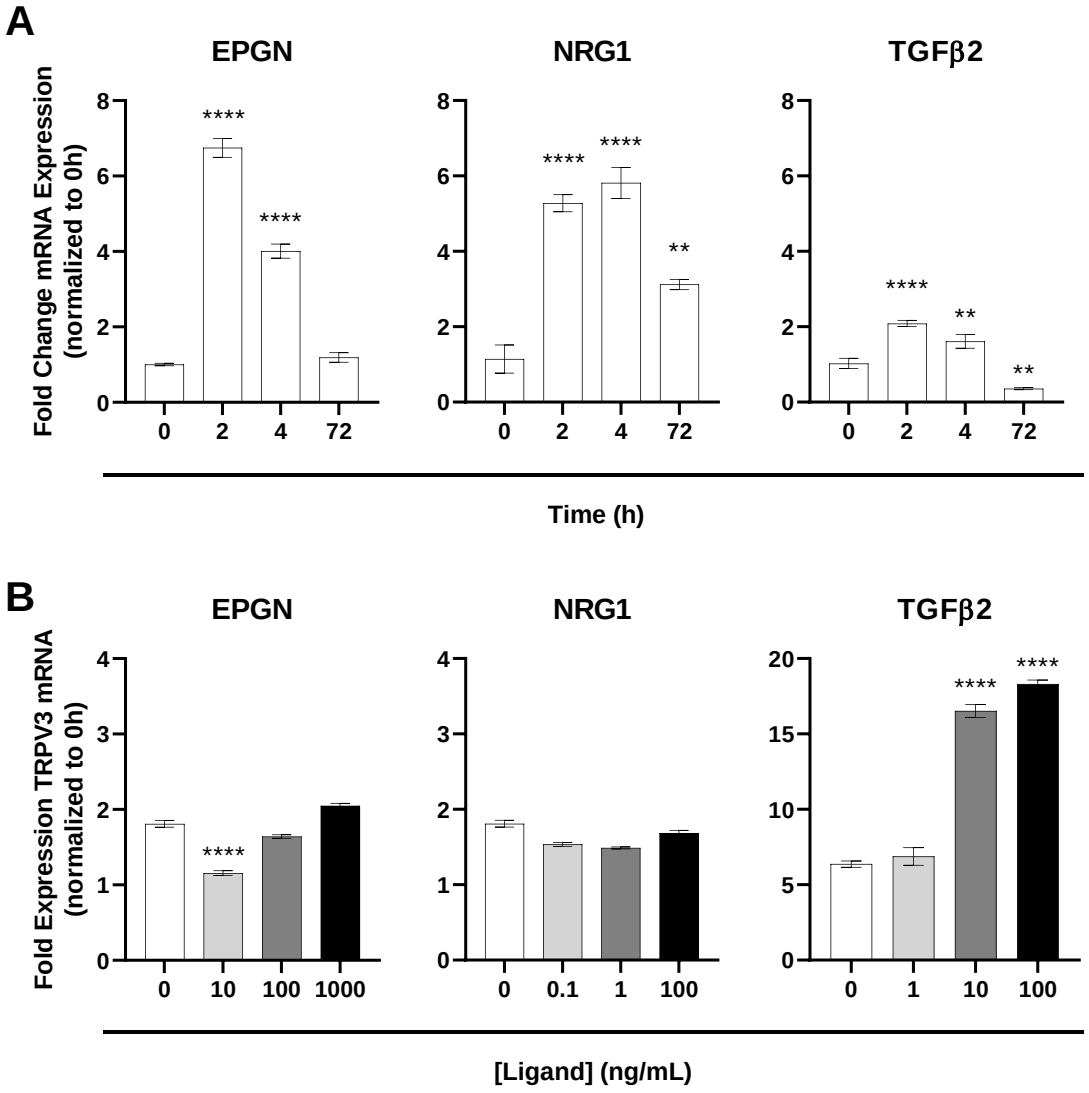

Supplemental Figure 5. A) Time-dependent induction of EPGN, NRG1 and TGFβ2 mRNA in HBEC3-KT cells compared to 0h confluent cells. **B)** TRPV3 mRNA induction 2h post-passaging injury with EPGN, NRG1 and TGFβ2 growth factor supplementation to conditioned media. Data were normalized to 0h, non-injured cells and presented as mean ± SD from $n \geq 3$ replicates. Significance was determined using one-way ANOVA with the Dunnett post-test. *$p < 0.05$, **$p < 0.01$, ***$p < 0.001$, ****$p < 0.0001$.

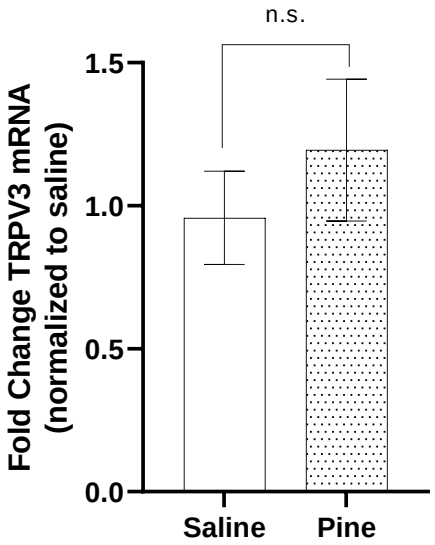

Supplemental Figure 6. *Trpv3* mRNA expression in distal airway/parenchymal tissue isolated from C57/BL6 mice treated sub-acutely with saline or 0.5 mg/kg pine PM via OPA. Data represent the mean ± SD from $n \geq 3$ for each treatment and significance was determined using an unpaired t-test setting $p < 0.05$ as the level for significance.

	Uninjured/100% Confluent (0h, Normalized)	Cell Passaging	Trypsin	Mechanical/Scratch Wound	Pine PM
HBEC3-KT	1.0 ± 0.1	**25.9 ± 0.3**	**11 ± 1**	*4.0 ± 0.7*	**20 ± 2**
BEAS-2B	1.1 ± 0.2	**42.3 ± 0.9**	1.9 ± 0.6	**6.3 ± 0.6**	**16 ± 1**
B2BV3OE	1.00 ± 0.08	3.0 ± 0.2	----	----	----
Lobar Bronchial	1.00 ± 0.03	*3.89 ± 0.06*	----	----	**6 ± 1**

Supplemental Table 1. Induction of TRPV3 mRNA in multiple human airway epithelial cell lines 2h after various types of *in vitro* injury. Data represent the mean ± SD from $n \geq 3$ for each injury model and are normalized to the confluent control of each cell line. Statistical significance was determined using two-way ANOVA with the Tukey post-test. $p < 0.05$ (values in *italics*), ****$p < 0.0001$ (values in **bold**).

Movie S1 (separate file). Videos showing the mechanical/scratch wound repair process for BEAS-2B (left) and B2BV3OE (right) cells over a period of 36h.

Movie S2 (separate file). Videos comparing the mechanical/scratch wound repair process for HBEC3-KT cells treated with media (vehicle, left) and the TRPV3 antagonists 007(300 μM, middle) or 008 (300 μM, right).

Movie S3 (separate file). Videos showing the mechanical/scratch wound repair process for HBEC3-KT cells treated with media (vehicle, left) and the TRPV3 antagonists DPTHF (150 μM, right).